OXFORD GENETICS

GENETICS, 2023, 225(1), iyad126
https://doi.org/10.1093/genetics/iyad126
Advance Access Publication Date: 12 July 2023
Investigation

The *Caenorhabditis elegans* cullin-RING ubiquitin ligase CRL4^{DCAF-1} is required for proper germline nucleolus morphology and male development

Mohammad M. Rahman,[1,3,†] Riju S. Balachandran,[1,†] Jonathan B. Stevenson,[1] Youngjo Kim,[1,4] Rui B. Proenca,[2] Edward M. Hedgecock,[2] Edward T. Kipreos[1,*]

[1]Department of Cellular Biology, University of Georgia, Athens, GA 30602, USA
[2]Department of Biology, Johns Hopkins University, Baltimore, MD 21218, USA
[3]Present address: The Laboratory of Biochemistry and Genetics, The National Institute of Diabetes and Digestive and Kidney Diseases, The National Institutes of Health, Bethesda, MD 20892, USA
[4]Present address: Department of Integrated Biomedical Science and Soonchunhyang Institute of Medi-Bioscience, Soonchunhyang University, Cheon-an 31151, Republic of Korea

*Corresponding author: Department of Cellular Biology, University of Georgia, 120 Cedar Street, Athens, GA 30602, USA. Email: ekipreos@uga.edu
[†]These authors contributed equally.

Abstract

Cullin-RING ubiquitin ligases (CRLs) are the largest class of ubiquitin ligases with diverse functions encompassing hundreds of cellular processes. Inactivation of core components of the CRL4 ubiquitin ligase produces a germ cell defect in *Caenorhabditis elegans* that is marked by abnormal globular morphology of the nucleolus and fewer germ cells. We identified DDB1 Cullin4 associated factor (DCAF)-1 as the CRL4 substrate receptor that ensures proper germ cell nucleolus morphology. We demonstrate that the *dcaf-1* gene is the *ncl-2* (abnormal nucleoli) gene, whose molecular identity was not previously known. We also observed that CRL4^{DCAF-1} is required for male tail development. Additionally, the inactivation of CRL4^{DCAF-1} results in a male-specific lethality in which a percentage of male progeny arrest as embryos or larvae. Analysis of the germ cell nucleolus defect using transmission electron microscopy revealed that *dcaf-1* mutant germ cells possess significantly fewer ribosomes, suggesting a defect in ribosome biogenesis. We discovered that inactivation of the sperm-fate specification gene *fog-1* (feminization of the germ line-1) or its protein-interacting partner, *fog-3*, rescues the *dcaf-1* nucleolus morphology defect. Epitope-tagged versions of both FOG-1 and FOG-3 proteins are aberrantly present in adult *dcaf-1(RNAi)* animals, suggesting that DCAF-1 negatively regulates FOG-1 and FOG-3 expression. Murine CRL4^{DCAF-1} targets the degradation of the ribosome assembly factor periodic trptophan protein 1 (PWP1). We observed that the inactivation of *Caenorhabditis elegans* DCAF-1 increases the nucleolar levels of PWP1 in the germ line, intestine, and hypodermis. Reducing the level of PWP-1 rescues the *dcaf-1* mutant defects of fewer germ cell numbers and abnormal nucleolus morphology, suggesting that the increase in PWP-1 levels contributes to the *dcaf-1* germline defect. Our results suggest that CRL4^{DCAF-1} has an evolutionarily ancient role in regulating ribosome biogenesis including a conserved target in PWP1.

Keywords: ribosome biogenesis, nucleolus, germ cell, DCAF1, male tail, male lethality

Introduction

The nucleolus is the most prominent compartment in the nucleus and is formed around the ribosomal DNA (rDNA) repeats (Hori et al. 2023). It is a membrane-free organelle that is the site of ribosome biogenesis, which constitutes ribosomal DNA (rDNA) transcription, ribosomal RNA (rRNA) processing, and ribosome assembly. The total number of ribosomes produced in a cell is related to its metabolic activity. Increases in ribosome production precede the initiation of DNA synthesis and mitosis during the cell cycle (Reddan and Unakar 1976). Disruption in nucleolar function impairs ribosome synthesis and halts the cell cycle (Chen et al. 2007; Lindstrom et al. 2007). In addition to mediating ribosome biogenesis, the nucleolus serves as a repository for dormant RNA and proteins that are involved in cell cycle progression, DNA repair, and telomere extension (Iarovaia et al. 2019). The size of the nucleolus is determined by the state of ribosome biogenesis (Derenzini et al. 2000; Uppaluri et al. 2016).

The cullin-RING ubiquitin ligase 4 (CRL4) is known to regulate fundamental cellular processes, including the cell cycle, transcription, and embryonic development (Jackson and Xiong 2009). CRL4 complexes recruit target substrates for ubiquitination and subsequent degradation by the 26S proteasome. The CRL4 complex consists of the scaffold protein CUL4 (cullin 4), the adaptor protein DDB1 (UV-damaged DNA binding protein 1), the RING finger protein Roc1/Roc2, and a variable substrate receptor (SR) that contains WD40 repeats (Jackson and Xiong 2009). CRL4 SRs are collectively known as DCAF (DDB1 Cullin4 associated factor). The binding of each unique DCAF SR to the core CRL4 components creates a different CRL4 ubiquitin ligase that targets different

Received: June 08, 2023. **Accepted:** July 02, 2023

substrates in response to different cellular and developmental cues (Zhou et al. 2020).

Characterization of CRL4 and its components in the nematode *C. elegans* revealed that mutants of the adaptor protein DDB-1 have a germ cell nucleolus morphology defect (Kim and Kipreos 2007a). The *ddb-1* mutant germ cell nucleoli are multilobed and irregular in shape. While inactivation of the CRL4 scaffold protein CUL-4 causes an early larval-stage arrest, *ddb-1* mutants develop to become sterile adults, presumably from the perdurance of DDB-1 maternal product that allows normal larval functions (Kim and Kipreos 2007a). The DCAF SR that is responsible for the nucleolus defect in *ddb-1* mutant germ cells was not known before this study.

Our current study identifies the *C. elegans* ortholog of human DCAF1 as the SR for the CRL4 complex, the loss of which is responsible for the germ cell nucleolus defect and a reduction in the number of germ cells. We also describe that loss of $CRL4^{DCAF-1}$ activity produces defects in male tail development and a partially penetrant lethality of male embryos and larvae. We find that the nucleolus morphology defect is associated with a reduction in ribosome numbers. We identify 3 genes whose inactivation rescues the germline nucleolus morphology defect: the ribosome assembly factor PWP-1; and the sperm fate specification mRNA-binding proteins FOG-1 and FOG-3.

Periodic trptophan protein 1 (PWP1) is a ribosome assembly factor that functions in pre-rRNA processing in budding yeast and human cells (Talkish et al. 2014; Han et al. 2020), and regulates the transcription of rRNA in *Drosophila* and human cells (Liu et al. 2017, 2018). A role for PWP1 in germ cells has not been reported previously.

The development of the *C. elegans* germ line is highly regulated. The gonad of a *C. elegans* hermaphrodite produces both oocytes and sperm for self-fertilization by spatiotemporal regulation of germ cells (Hubbard and Schedl 2019). Germline development is regulated by sets of proteins that control germ cell proliferation, the meiotic/mitotic decision, and sex determination (Hubbard and Schedl 2019). Many of the regulatory proteins involved in germline development are mRNA-binding proteins that regulate mRNA translation (Ellis 2022).

FOG-1 is a cytoplasmic polyadenylation element binding (CPEB) mRNA-binding protein (Ellis 2022). FOG-1 functions in a protein complex with the Tob/BTG family member FOG-3 (Ellis 2022). FOG-1 and FOG-3 are required for sperm formation in hermaphrodites and males (Barton and Kimble 1990; Ellis and Kimble 1995).

Adult *C. elegans* males differ structurally from hermaphrodites primarily in being thinner, having a different gonad shape, lacking a vulva, and having a tail that is specialized for copulation (Emmons 2005). Larval-stage cell divisions produce the cells that form the structures of the male tail, including the fan, sensory rays, spicules, and the proctodeum chamber, where the gut, vas deferens, and spicule channels come together (Emmons 2005).

Materials and methods

RNA interference (RNAi)

Feeding RNAi experiments used HT115 bacteria transformed with dsRNA expression clones in the plasmid pPD129.36 double-stranded RNA (dsRNA) expression vector (Timmons et al. 2001) for the majority of experiments. All RNAi clones used were from the Ahringer library (Poulin et al. 2004) except *pwp-1*. *pwp-1* RNAi was accomplished with a 759 bp genomic fragment cloned into the T444T plasmid (Sturm et al. 2018). The *pwp-1* fragment was cloned into T444T using the In-Fusion cloning kit (Takara Bio). The primers for cloning the *pwp-1* fragment, which includes 15 bp of overlap with the T444T cut with XbaI and Sma I restriction enzymes, are 5′ tggcggccgctctaG GTGACTTCACACTCGAGTGC 3′ and 5′ gaattcctgcagccC TCATCTTCGCCAACAGTAACC 3′. To inactivate *fog-1* by feeding RNAi, we cloned a 1215 bp fragment of *fog-1* cDNA into the pPD129.36 plasmid and expressed the plasmid in iOP50 bacteria (Neve et al. 2020). The *fog-1* cDNA sequence begins with ATGATGAATCGGAAGA and ends with TGTTAATAT GGGAAAG. Feeding RNAi experiments in Figs. 4b and c, 5, and 6 used iOP50 bacteria, while HT115 bacteria were used for other experiments.

dsRNA expression in the bacteria was induced with 1 mM IPTG for 4–6 hours (added at OD600 = 0.4–0.6 of logarithmic growth) when the bacteria were grown in 2xYT broth. Bacteria were spun down and concentrated before placement on 1xNGM plates with 1 mM IPTG and 100 µg/ml carbenicillin. For control RNAi experiments, HT115 or iOP50 transformed with empty vector pPD129.36 or T444T was used under similar experimental conditions.

Immunofluorescence

Gonad dissection was performed as previously described (Feng et al. 1999). Ten to twenty animals were placed into a drop of 10 µl of M9 buffered salt solution or M9 with 0.25 mM levamisole (to induce paralysis) onto a circled slide coated with 25 µl of poly-L-lysine solution (the slides with poly-lysine had been previously heated at 85°C for 30 minutes). A #15 scalpel was used to cut the animals posterior to the pharynx to release the gonad. A 24 × 60 mm no. 1.5 coverslip was added to the slides and the slide was frozen on a metal block cooled on dry ice. The coverslip was removed quickly, and the slide was processed for immunofluorescence as described previously for the detection of 3xMyc::FOG-1 and FOG-3::3xFLAG proteins (Noble et al. 2016). Rat anti-Myc antibody (JAC6, Bio-Rad) was used at a 1:300 dilution, and mouse anti-FLAG antibody (M2, Sigma) was used at a 1:1,000 dilution in blocking buffer. Secondary antibodies, anti-rat coupled to AlexaFluor 488 and anti-mouse IgG1 coupled to AlexaFluor 546 (Thermo Fisher, Waltham, MA, USA), were used at a 1:1,000 dilution. In all slides, DNA was stained with 1 µg/ml Hoechst 33258.

Microscopy and quantitation of fluorescence images

Images were taken using a Zeiss Axioscope microscope equipped either with a Hamamatsu ORCA-ER CCD camera controlled with OpenLab 5.5 software or with a Tucsen Dhyana 400BSI v2 sCMOS camera controlled with Micromanager software (version 1.4.23). Fluorescence images were taken at matched exposures for all samples; exposures were not saturating. Matching fluorescence images were processed identically using Adobe Photoshop (version 22) for figures.

Quantitation of fluorescence images was performed with Adobe Photoshop or ImageJ (version 1.51s). For quantitation of the level of 3xMyc::FOG-1 and FOG-3::3xFLAG in immunofluorescence images of dissected gonads, the Hoechst staining was used to demarcate the "distal" region as being distal to the transition zone, and the "proximal" region as including pachytene and more proximal regions of the gonad. Regions for quantitation were selected with a free-hand tool. The mean sample signal was taken in the appropriate region of the gonad and the mean background signal was taken from an empty region of approximately the same area next to the gonad. The mean sample signal minus the mean background signal was used for comparisons between samples. There was a low, background signal in the nucleus

of most images for wild-type control for anti-Myc staining, and the nucleoli for anti-FLAG staining.

For quantitation of wrmScarlet::PWP-1 levels, the mean sample signal minus the mean background signal was multiplied by the area (number of pixels) of the nucleolus to give a total signal for each nucleolus.

Analysis of dissected gonads for rRNA and ribosomal proteins

Isolated gonads were lysed with 1× SDS sample buffer for analysis with LC-MS/MS. LC-MS/MS was performed with an Orbitrap Fusion mass spectrometer (ThermoFisher), with subsequent label-free analysis using MaxQuant software (Cox et al. 2014) at the Emory Integrated Proteomics Core.

RNA extraction from isolated gonads was carried out using Trizol with the standard protocol (ThermoFisher). Extracted RNA was analyzed using the Agilent Bioanalyzer in the Georgia Genomics and Bioinformatics Core with RNA 6000 Pico analysis.

Timing of larval development

The timing of larval development was carried out at 25°C as this is the nonpermissive temperature for the *fog-1(q253ts)* allele. Pretzel-stage embryos for wild type, *pwp-1(ok3322)/nT1*, and *fog-1(q253ts)* were placed on plates of control or *dcaf-1* RNAi. After 3 hours, L1 larvae that hatched were kept on the plate, while eggs that had not hatched were removed. Plates were analyzed at hour intervals to score adults based on the protrusion of their vulvae, which is not observed in larvae. Upon counting adults, they were removed from the plates. The numbers of animals scored ranged from 13 to 28.

Statistics

Error bars are standard error of the mean (SEM). Student's *t*-test and χ^2 test were used to determine statistical significance; *P*-values: ns, not significant; * ≤ 0.05; ** ≤ 0.01; *** ≤ 0.001; **** ≤ 0.0001. In graphs, asterisks above bars denote comparisons to the relevant control; asterisks above lines denote comparisons under the lines.

Supplementary Methods contains a list of the *C. elegans* strains used and other methods.

Results

$CRL4^{DCAF-1}$ inactivation causes a germ cell nucleolus morphology defect

Homozygous mutants of the CRL4 adaptor protein, *ddb-1(tm1769)*, are sterile hermaphrodites with a germ cell nucleolar morphology defect (Kim and Kipreos 2007a) (Fig. 1a). Somatic blast cells in *cul-4* or *ddb-1* mutants undergo re-replication to generate increased DNA content, due to the failure to properly regulate the DNA replication-licensing factors CDT-1 and CDC-6 (cell division cycle related-6) (Zhong et al. 2003; Kim et al. 2007; Kim and Kipreos 2007a). In contrast to the phenotype in somatic cells, *ddb-1* mutant germ cells do not exhibit significantly increased DNA content in germ cells, as quantified previously (Kim and Kipreos 2007a) (Supplementary Fig. 1).

In order to identify the SR that functions to maintain proper germ cell nucleolus morphology, we performed an RNAi screen of 9 genes that are orthologs of known CRL4 SRs in other species to determine if any phenocopied the *ddb-1* germline defect. Of the 9 genes tested, only RNAi depletion of ZK1251.9 resulted in sterility and phenocopied the *ddb-1* mutant germ cell nucleolus morphology defect (Supplementary Table 1; Fig. 1b). ZK1251.9 is orthologous to the mammalian CRL4 SR DCAF1/VprBP (Nakagawa et al. 2013). The 2 proteins share 68% similarity and 33% identity (Supplementary Fig. 2) and reciprocally identify each other with BLAST searches at e-values of 0.0 in each direction. To reflect this orthology, we named the ZK1251.9 gene *dcaf-1*.

To confirm the nucleolus defect in *dcaf-1(RNAi)* germ cells, we utilized a previously published nucleolus-specific reporter, nucleostemin translational fusion with GFP (NST-1::GFP) (Kudron and Reinke 2008). NST-1::GFP has a similar nucleolar localization in *dcaf-1(RNAi)* germ cells compared to control(RNAi) germ cells, but the irregular pattern matches the DIC images (Supplementary Fig. 3).

To analyze DCAF-1 function, we used the *dcaf-1(ok1867)* deletion allele provided by the *C. elegans* Gene Knockout Consortium, which we outcrossed 6 times. The *ok1867* allele comprises a large 1.2 kb deletion that introduces a frameshift that generates a premature stop codon (Fig. 1c; Supplementary Fig. 2). The *ok1867* mutation eliminates 45% of the coding sequence (losing amino acids 759 to 1701), including the 7 WD40 repeats. The predicted truncated protein is 790 amino acids in length (with 758 N-terminal amino acids of wild-type DCAF-1). The homozygous *dcaf-1(ok1867)* mutant demonstrates the same germline nucleolus morphology defect as observed with *dcaf-1* RNAi (Fig. 1b). Similar to *ddb-1* mutants, the nucleolar morphology defect affects a majority of germ cells in both larval-stage and adult *dcaf-1* mutants.

Similar to *ddb-1(tm1769)* homozygous mutants, *dcaf-1(ok1867)* homozygous mutants generated from a heterozygous mother develop into sterile adults. *dcaf-1(ok1867)* have reduced numbers of germ cells, and the majority of *dcaf-1* mutant adults do not produce sperm (74%, $n = 22$) or oocytes (77%, $n = 13$), as assessed with fluorescent markers for sperm (*spe-11p*::mCherry) and oocytes (*rme-2p*::RME-2::GFP). Other mutant phenotypes of the *dcaf-1(ok1867)* mutants or RNAi depletion are protruding vulva (63% at 20°C; 80% at 25°C, $n = 30$ each) and slow growth (100%, $n = 14$; Fig. 6c). The germ cell nucleolus morphology defect in *dcaf-1* mutants can be observed as early as the L1 stage (Fig. 6a). We did not observe obvious nucleolus morphological defects in somatic tissues, including hypodermis, vulva, and intestine (data not shown).

Heterozygous *dcaf-1(ok1867)* mutants exhibit a reduced brood size at 20°C, which was 27% of that of the wild type (Supplementary Fig. 4). At the higher temperature of 26°C, ~50% of the *dcaf-1* heterozygotes were sterile (compared to no sterility in wild type, $n = 20$ each). Thus, heterozygous *dcaf-1* mutants have a reduction in brood size at 20°C and increased sterility at 26°C.

We tested whether DCAF-1 is required for embryonic development. We placed *dcaf-1(ok1867)* heterozygous L4-stage larvae (P0) on *dcaf-1* feeding RNAi, and analyzed the F1 generation. Homozygous *dcaf-1* F1 animals generated from heterozygous mothers subject to *dcaf-1* RNAi would lack both maternal and zygotic *dcaf-1*. No embryonic lethality was observed when animals were raised at various temperatures (16°C, 20°C, or 25°C); and all F1 animals that hatched on *dcaf-1* RNAi developed into sterile adults with the same germ cell nucleolus morphology defect as *dcaf-1* mutants not subject to RNAi (data not shown). These results suggest that DCAF-1 is not essential for embryonic development.

The *ncl-2* gene is *dcaf-1*

In 1983, the *ncl-2* (abnormal nucleolus) mutation was isolated by one of us (E.M.H.) based on its striking germ cell nucleolus morphology defect. *ncl-2* has only a single reported allele, *e1896*. The *ncl-2(e1896)* germ cell phenotype is identical to that of *dcaf-1(ok1867)* mutants (Fig. 1b). The *ncl-2* gene had not been molecularly

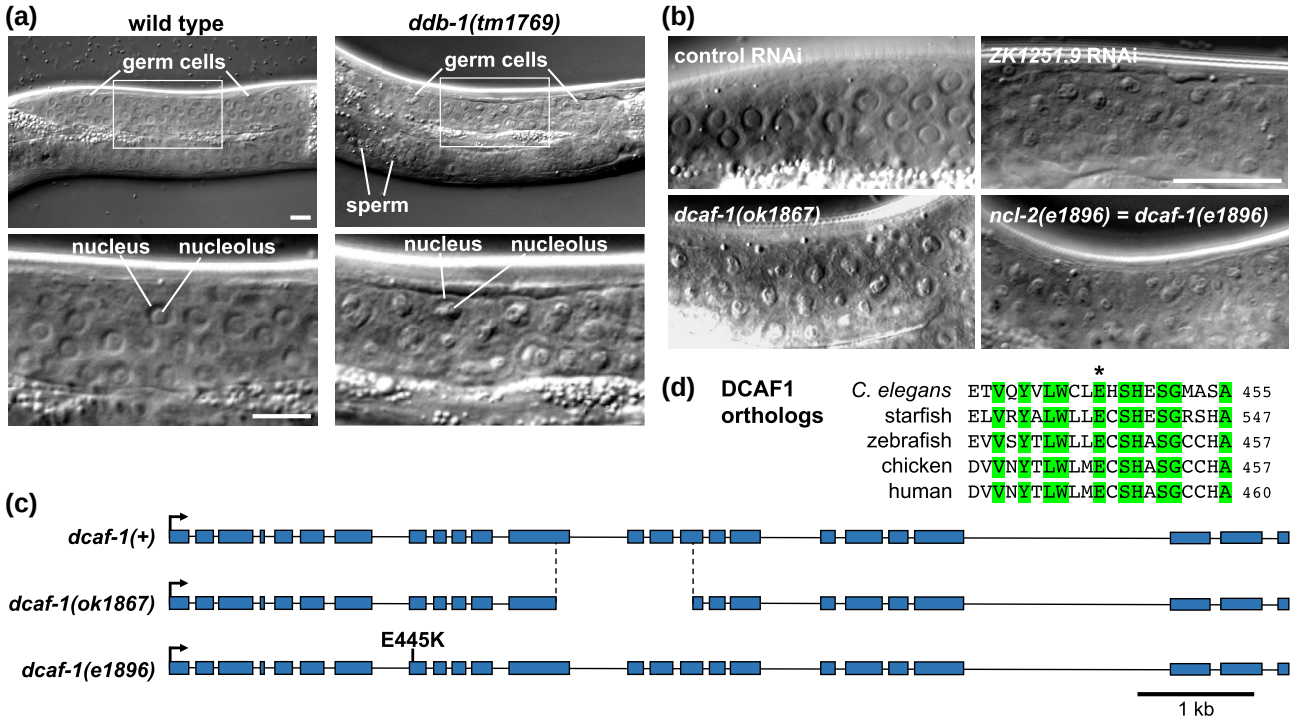

Fig. 1. *dcaf-1* inactivation phenocopies the *ddb-1* mutant germline nucleolus defect. a) DIC images of one gonad arm for wild type and *ddb-1(tm1769)* mutant. The boxed region in the upper image is shown at higher magnification in the bottom image. b) DIC images of germ cells in control RNAi, ZK1259.1 (*dcaf-1*) RNAi, *dcaf-1(ok1867)*, and *ncl-2(e1896)*. Note that the 3 methods of inactivating *dcaf-1* phenocopy the *ddb-1* mutant germ cell nucleolus morphology defect. Scale bars, 10 μm. c) Schematic of the *dcaf-1* genomic locus (exons are boxes and solid lines are introns). The region deleted in the *dcaf-1(ok1867)* mutant is between the dotted lines. The location of the *dcaf-1(e1896)* missense mutation that gives rise to the E445K protein change is marked. d) An alignment of the region flanking the E445K mutation (marked by an asterisk) in allele *e1896* for orthologs in several diverse animal species (*Asterias rubens*, *Danio rerio*, *Gallus domesticus*, and *Homo sapiens*). Residues that are conserved in all of the species are shaded.

identified. We mapped the *ncl-2* gene to the same region on chromosome IV that contains the *dcaf-1* gene. A complementation test between the 2 alleles revealed that *dcaf-1(ok1867)* does not complement *ncl-2(e1896)*, suggesting that the mutations are in the same gene. Sequencing the *dcaf-1* gene in the *ncl-2(e1896)* mutant identified a point mutation (G1333A) in the *dcaf-1* coding region that changes an acidic glutamic acid residue (E) to a basic lysine residue (K) at amino acid position 445 (Fig. 1c). The mutated E residue is evolutionarily conserved, being present in diverse animal DCAF-1 orthologs (Fig. 1d). Thus, we conclude that *ncl-2* and *dcaf-1* are the same gene.

DCAF-1 is required for normal ribosome numbers in the germ line

The germ cell nucleolus of *dcaf-1* homozygous mutants is abnormal in size, multilobed, and irregular in shape (Fig. 1b). Transmission electron microscopy (TEM) micrographs of distal-arm germ cells of *dcaf-1(e1896)* mutants show the nucleolus defect at higher resolution. Changes in the shape of the nucleolus are visible in *dcaf-1(e1896)* germ cells relative to wild type (Fig. 2a–d). Magnification of the nucleolus in wild-type germ cells shows regions of assembled ribosome subunits and other regions devoid of assembled subunits (Fig. 2b′). In the *dcaf-1(e1896)* nucleolus, assembled ribosomes of the correct size are not observed at normal levels. Instead, there is often a segregation of regions without subunits and regions with large aggregates that are larger than the assembled ribosomes observed in the wild type (Fig. 2d′).

The cytoplasm of *dcaf-1(e1896)* germ cells has decreased numbers of ribosomes when compared to the wild type (Fig. 2b″ and d″). The *dcaf-1(e1896)* mutant germ cells have 20 ± 5.4 ribosomes per arbitrary square of cytoplasm, while wild-type germ cells have 58 ± 7.7 (Fig. 2g). This reflects significantly fewer ribosomes in the germ line of *dcaf-1* mutants (34% of the wild-type level). Thus, there is a defect in ribosome numbers in the germ line of *dcaf-1* mutants.

Analysis of somatic hypodermal cells showed that there is not an obvious difference in the morphology of nucleoli or the number of ribosomes in the cytoplasm between *dcaf-1(e1896)* mutants and wild type (Fig. 2e, e″, f, f″, g). These results (coupled with DIC observations of other tissues) suggest that the *dcaf-1* mutant defect in ribosome numbers and nucleolar morphology is largely absent from somatic tissues.

To determine if the levels of ribosomal proteins in the germ line were altered significantly in *dcaf-1(RNAi)* animals, we analyzed the relative number of ribosomal proteins in dissected gonads from control(RNAi) and *dcaf-1(RNAi)* adults. Gonads were dissected and collected, lysed, run on SDS-PAGE, and then subjected to tryptic digest, with the peptides analyzed by liquid chromatography coupled to liquid chromatography tandem mass spectrometry (LC-MS/MS). Label-free protein quantification (Cox et al. 2014) was used to assess the levels of ribosomal proteins in *dcaf-1(RNAi)* vs control(RNAi) gonads. Only 5 ribosomal proteins were altered by close to 2-fold, with increases observed for large ribosomal subunit-15A (RPL-15A), RPL-36.A, and small ribosomal subunit-30 (RPS-30), and decreases for RPL-31 and RPS-29 (Supplementary Fig. 5a). Other ribosomal proteins had smaller changes in level upon *dcaf-1* RNAi. The majority of the changes were decreases rather than increases in level (30 vs 11 for large ribosomal proteins; and 17 vs 8 for small ribosomal proteins).

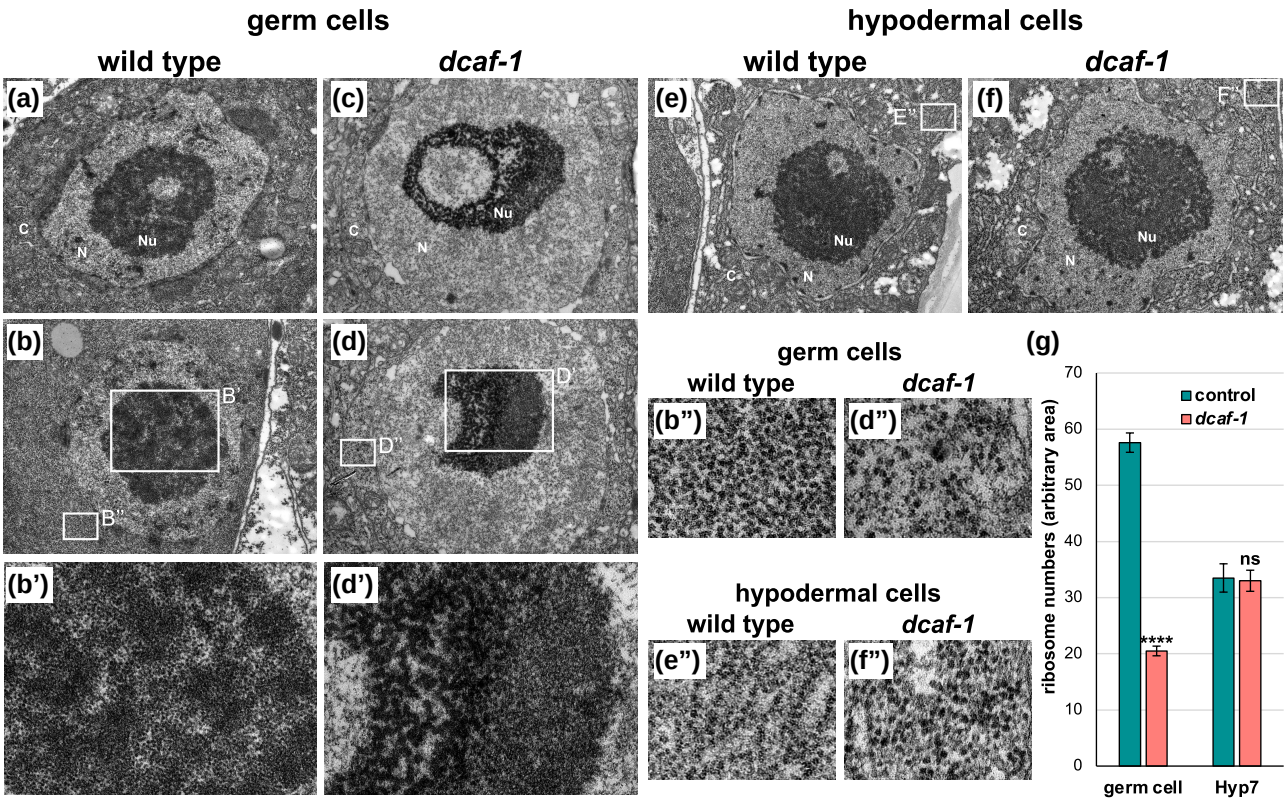

Fig. 2. Transmission electron micrographs of *dcaf-1* mutant germ cells and hypodermal cells. a–d) Micrographs of wild type and *dcaf-1*(*e1896*) mutant germ cells in the distal region of the gonad. Panels b′ and d′) show the larger-boxed regions in panels B and D at higher magnification. Nu, nucleolus; N, nucleus; C, cytoplasm. e and f) Micrographs of wild type and *dcaf-1*(*e1896*) mutant hypodermal cells in the Hyp7 syncytium. Panels b″, d″, e″, and f″) show the smaller-boxed regions of panels b, d, e, and f) at higher magnification. g) Graph of the number of ribosomes per arbitrary area in germ cells and hypodermis (Hyp7) of wild type and *dcaf-1*(*e1896*) mutants; $n = 20$ counts for each condition except for germ cells in *dcaf-1*(*e1896*) mutants that had 40 counts. ns, not significant; ****P-value <0.0001. Statistics are comparisons to the appropriate wild-type control. Throughout, error bars are SEM.

The correct processing of pre-rRNA to generate 5.8S, 18S, and 28S rRNAs is important to prevent defects in ribosome biogenesis (Henras et al. 2008). To determine if the relative steady-state levels of 18S and 28S rRNAs are altered by the inactivation of DCAF-1, we extracted RNA from gonads of animals treated with control or *dcaf-1* RNAi and quantitated rRNA levels using a bioanalyzer. We found that the relative levels of the 2 major rRNA transcripts were not significantly different in *dcaf-1*(*RNAi*) gonads compared to control(RNAi) gonads (Supplementary Fig. 5b, c). While the relative levels of rRNA were similar, the overall rRNA level was lower for the *dcaf-1*(*RNAi*) gonads. This can be attributed to using the same number of gonads for each sample, but *dcaf-1*(*RNAi*) gonads have significantly fewer germ cells, and therefore are expected to produce less rRNA per gonad.

dcaf-1 and *cul-4* mRNA are enriched in the hermaphrodite germ line (Reinke et al. 2004; Kim and Kipreos 2007a; Wang et al. 2009). To determine whether DCAF-1 functions within germ cells to regulate their nucleolus morphology, we utilized a strain in which RNAi is effective in the germ line but ineffective in multiple somatic tissues, including the somatic gonad (Zou et al. 2019). This strain contains a *rde-1* (RNAi-defective 1) null mutant that expresses RDE-1 in the germ line. Because the Argonaute protein RDE-1 is required for RNAi to occur, only the germ line has functional RNAi. *dcaf-1* RNAi depletion in this strain conferred a 100% penetrance of the germ cell nucleolus morphology defect (Table 1). This suggests that DCAF-1 normally functions in the germ line to promote proper nucleolus morphology and germ cell proliferation.

DCAF-1 is required for male tail morphology and viability

After self-mating of male and hermaphrodite *dcaf-1*(*ok1867*)/*nT1* heterozygotes, few *dcaf-1*/*dcaf-1* homozygous males were observed relative to *dcaf-1*/*nT1* heterozygous males: 5 *dcaf-1*/*dcaf-1* males vs 218 *dcaf-1*/*nT1* males. Given 218 *dcaf-1*/*nT1* heterozygous males, 109 *dcaf-1*/*dcaf-1* males are expected. A similar dearth of *ddb-1*/*ddb-1* males was obtained from self-mating *ddb-1*/*nT1* heterozygotes: 14 *ddb-1*/*ddb-1* males vs 509 *ddb-1*/*nT1* males. Thus, only 4.6 and 5.5% of the expected *dcaf-1*/*dcaf-1* and *ddb-1*/*ddb-1* males were observed, respectively, with the difference significant with χ^2 P-values of 9.9×10^{-23} and 4.6×10^{-48}. The lack of males with both mutations of *dcaf-1* and *ddb-1* implies that the phenotype is attributable to the loss of the $CRL4^{DCAF\text{-}1}$ complex.

Males can only be unambiguously identified using a stereomicroscope at the L4 and adult stages. To determine when *dcaf-1*/*dcaf-1* or *ddb-1*/*ddb-1* males arrest, we picked L1 larvae onto their own plates one day after self-mating of *dcaf-1*/*nT1* and *ddb-1*/*nT1* heterozygotes. The L1 larvae were scored for genotype (based on pharyngeal GFP expression linked to *nT1*) and for sex when the animals were at the L4 or adult stages (Tables 2 and 3). *nT1*/*nT1* animals are not present because the homozygous translocation is embryonic lethal. We observed significantly less *dcaf-1*/*dcaf-1* males (1 of 12 expected) and *ddb-1*/*ddb-1* males (0 of 18 expected). The missing homozygous males could not be attributed to arrested or missing larvae because none of the homozygous larvae were arrested or missing. Further, homozygous males were unlikely to be incorrectly assigned as hermaphrodites because

Table 1. Suppression screen for *dcaf-1* germ cell nucleolus morphology defect.

Strain	RNAi	Suppression of *dcaf-1* germline defect	*n* (number of animals)
N2 wild type	Vector	NA	20
N2 wild type	*ddb-1*	No	20
N2 wild type	*dcaf-1*	No	20
dcaf-1(ok1867)	Vector	No	15
dcaf-1(ok1867)	*cki-1*	No	15
dcaf-1(ok1867)	*cdt-1*	No	15
rde-1(mkc36); sun-1p::RDE-1	*dcaf-1*	No	16
Nucleolus regulator			
ncl-1(e1865)	*dcaf-1*	No	15
Cell cycle regulators			
cki-1(gk132)	*ddb-1*	No	15
gmn-1(tm2212)	*ddb-1*	No	15
lin-35(n745)	*dcaf-1*	No	15
Checkpoint regulators			
chk-1(tm938)	*dcaf-1*	No	15
atl-1(tm853)	*dcaf-1*	No	15
atm-1(gk186)	*dcaf-1*	No	15
Cell death regulators			
cep-1(w40)	*dcaf-1*	No	15
cep-1(gk138)	*dcaf-1*	No	15
cep-1(ep347)	*dcaf-1*	No	15
ced-3(n1286)	*dcaf-1*	No	15
ced-3(n717)	*dcaf-1*	No	15
Germ cell proliferation			
glp-1(e2141)	*dcaf-1*	No	15
glp-1(ar202gf)	*dcaf-1*	No	15
gld-3(q741)	*dcaf-1*	No	10
gld-3(q730)	*dcaf-1*	No	10
gld-3(ok308)	*dcaf-1*	No	10
gld-3(q730);nos-3(q650)	*dcaf-1*	No	15
Mitotic/meiotic fate decision			
fbf-1(ok91)	*dcaf-1*	No	15
fbf-1(ok91); fbf-2(q704)	*dcaf-1*	No	15
Sex-determination pathway			
qDf4/+ het [deletes *fog-1*]	*dcaf-1*	Partial (41%)[a]	44
fog-1(q325)	*dcaf-1*	Partial within gonad[b]	15
fog-1(q372)	*dcaf-1*	No	10
fog-1(e2121)	*dcaf-1*	Partial (75%)	15
fog-1(q253ts); 25°C	*dcaf-1*	**Yes**	15
fog-1(q241)	*dcaf-1*	Partial within gonad[b]	10
dcaf-1(ok1867)	*fog-1*	**Yes**	10
fog-3(q470)	*dcaf-1*	Partial (33%)	9
fog-3(q443)	*dcaf-1*	Partial (40%)	25
dcaf-1(ok1867)	*fog-3*	Partial (10%)	10
fem-3(e2006ts); 25°C	*dcaf-1*	No	15
tra-1(e1488)	*dcaf-1*	No	15
tra-1(e1099)	*dcaf-1*	No	10
tra-1(e1575)/+ [gain-of-function]	*dcaf-1*	No	20
Ribosome assembly factor			
pwp-1(ok3322)	*dcaf-1*	**Yes**	20
pwp-1(ok3322)/+ [heterozygote]	*dcaf-1*	Partial (60%)	20
dcaf-1	*pwp-1: control*	Partial (93%)	15

[a] Partial rescue gives the percentage of animals with no nuclear morphology defects or only a small percentage of germ cells with defects.
[b] Germ cell nucleolus defect was suppressed in the proximal but not distal region of the gonad.

homozygous hermaphrodites were not overrepresented. Thus, the *dcaf-1*/*dcaf-1* and *ddb-1*/*ddb-1* males were presumably not present because they were arrested as embryos before the L1 larval stage that was picked.

Because *dcaf-1*/*nT1* animals generate 11/16 arrested embryos (due to imbalanced translocation chromosomes and *nT1*/*nT1* lethality), it was not possible to analyze the number of arrested embryos due to *dcaf-1* male lethality. To allow an analysis of embryonic arrest, we created a *dcaf-1* strain with a nonlethal balancer mutation, *lron-14(gk5340)*, which is only 0.07 map units from *dcaf-1*. The *lron-14(gk5340)* mutation is an insertion in the *lron-14* gene that introduces a transgene for GFP expression in the pharynx (Au et al. 2019). *lron-14* loss-of-function does not have any reported phenotypes (www.wormbase.org).

The eggs from a *dcaf-1*/*lron-14(gk5340)* self-cross were analyzed for arrest, and hatched larvae were scored for genotype (based on pharyngeal GFP signal) and sex (Table 4). 52% of the expected *dcaf-1*/*dcaf-1* males were observed relative to the expected number (34 males observed and 65 expected). Seven *dcaf-1*/*dcaf-1* larvae were arrested before their sex could be assessed. Additionally, there were 28 arrested eggs. Adding the number of *dcaf-1*/*dcaf-1* arrested eggs (28) and arrested larva (7) to the number of *dcaf-1*/*dcaf-1* males observed (34) makes up the deficit relative to the expected numbers of males (65). Notably, a control group of unmated *dcaf-1*/*lron-14*(gk540) showed that none of their eggs were arrested (0 of 260). The difference in arrested eggs between the progeny of *dcaf-1*/*lron-14* that were mated (28 of 500) vs unmated (0 of 260) was significant with the χ^2 test at $P < 0.0001$. Males arise spontaneously at a rate of ~1 in 500 (Hodgkin 1983), and thus less than one is expected for 260 unmated progeny. Thus, the increase in arrested *dcaf-1*/*dcaf-1* eggs in the mated progeny can be attributed to the arrest of male embryos.

Table 2. *dcaf-1*/*dcaf-1* male progeny from cloned L1 from *dcaf-1*/*nT1* self-cross.

Genotype	Sex or arrest/ missing	Number	Notes	*P*-value
dcaf-1/nT1	Hermaphrodite	48		
dcaf-1/nT1	Male	34	Implies 70.8% cross-progeny (34/48)	
dcaf-1/nT1	Arrested larvae	6		
dcaf-1/nT1	Missing	4		
dcaf-1/dcaf-1	Hermaphrodite	17	24 expected relative to het (48/2)	ns
dcaf-1/dcaf-1	Male	1	12 expected relative to herm. (17 × 0.708)	<0.01*
dcaf-1/dcaf-1	Arrested larvae	0		
dcaf-1/dcaf-1	Missing	0		

Table 3. *ddb-1*/*ddb-1* male progeny from cloned L1 from *ddb-1*/*nT1* self-cross.

Genotype	Sex or arrest/ missing	Number	Notes	*P*-value
ddb-1/nT1	Hermaphrodite	56		
ddb-1/nT1	Male	40	Implies 71.4% cross-progeny (40/56)	
ddb-1/nT1	Arrested larvae	9		
ddb-1/nT1	Missing	0		
ddb-1/ddb-1	Hermaphrodite	25	28 expected relative to het (56/2)	ns
ddb-1/ddb-1	Male	0	18 expected relative to herm. (25 × 0.714)	<0.001
ddb-1/ddb-1	Arrested larvae	0		
ddb-1/ddb-1	Missing	0		

Table 4. *dcaf-1*/*dcaf-1* male progeny from cloned embryos from *dcaf-1*/*lron-14* self-cross.

Genotype	Sex or arrest/ missing	Number	Notes	P-value
dcaf-1/*lron-14*	Hermaphrodite	119		
dcaf-1/*lron-14*	Male	112	Implies 94% cross-progeny (112/119)	
dcaf-1/*lron-14*	Arrested larvae	0		
dcaf-1/*lron-14*	Missing	0		
lron-14/*lron-14*	Hermaphrodite	71	60 expected relative to het (119/2)	ns
lron-14/*lron-14*	Male	60	67 expected relative to herm. (71 × 0.94)	ns
lron-14/*lron-14*	Arrested larvae	0		
lron-14/*lron-14*	Missing	0		
dcaf-1/*dcaf-1*	Hermaphrodite	69	60 expected relative to het (119/2)	ns
dcaf-1/*dcaf-1*	Male	34	65 expected relative to herm. (69 × 0.94)	<0.01
dcaf-1/*dcaf-1*	Arrested larvae	7		
dcaf-1/*dcaf-1*	Missing	0		
Arrested eggs		28		

There was a significantly lower percentage of observed vs expected adult *dcaf-1*/*dcaf-1* male progeny from a *dcaf-1*/*nT1* self-cross (~6–8%) compared to a *dcaf-1*/*lron-14* self-cross (~50%). This suggests that the genetic background of the parent impacts the viability of male *dcaf-1* embryos.

dcaf-1 and *ddb-1* males have the same stereotypical germline nucleolus defect that is observed in *dcaf-1* and *ddb-1* hermaphrodites (Fig. 3a). The percentage of adult males that produce sperm is reduced in *dcaf-1* (27%, $n = 15$) and *ddb-1* (9%, $n = 11$) mutants. Additionally, there is a severe and fully penetrant defect in the morphology of the male tail in *dcaf-1* and *ddb-1* mutants (Fig. 3b). The defective development of the male tail generally affects the connection of the gut to the exterior, and *dcaf-1* and *ddb-1* males are usually constipated.

Potential suppressors of the *dcaf-1* nucleolus morphology defect

In order to gain further insights into the germline defect in *dcaf-1* mutants, we tested candidate genes for suppression of the *dcaf-1* loss-of-function phenotype in hermaphrodites (Table 1). We did not observe rescue of the *dcaf-1* RNAi nucleolus phenotype by inactivation of genes that inhibit the cell cycle and so could have potentially contributed to the reduction in germ cell numbers in *dcaf-1(RNAi)* animals (*cki-1*, *gmn-1*, and *lin-35*) (Kipreos and van den Heuvel 2019). A rescue was not observed for the inactivation of cell cycle checkpoint genes whose activity could have potentially contributed to the reduction in germ cell numbers in *dcaf-1(RNAi)* animals (*chk-1*, *atl-1*, and *atm-1*) (Gartner and Engebrecht 2022). A rescue was not observed for inactivating genes required for apoptosis in the germ line or more broadly (*cep-1* and *ced-3*) (Gartner et al. 2008). A rescue was not observed for alleles that impact mitotic germ cell division, either promoting division (*glp-1(ar202)*, and *gld-3*; *nos-3*) or inhibiting division (*glp-1(e2141)*) (Hubbard and Schedl 2019). Finally, rescue was not observed for inactivation of genes that regulate the meiotic/mitotic decision (*fbf-1* and *fbf-2*) (Ellis 2022).

Inhibition of RNA Pol I-mediated transcription in mouse embryonic fibroblasts causes nucleolus disruption, a ribosome biogenesis defect, and a reduction in assembled ribosomes leading to cell growth arrest (Yuan et al. 2005). We tested whether increased RNA Pol I mediated transcription of rRNA could rescue the nucleolus morphology defect in *dcaf-1* mutant germ line. Mutations in the *ncl-1* gene, which encodes a repressor of RNA Pol I- and RNA Pol III-mediated transcription, results in excessive rRNA and 5S RNA transcription and enlargement of nucleoli in *C. elegans* cells (Frank and Roth 1998). Additionally, LIN-35/Rb is also reported to negatively regulate rRNA transcription in *C. elegans* cells (Voutev et al. 2006). We inactivated *dcaf-1* by RNAi in *ncl-1(e1865)* and *lin-35(n745)* mutants and observed that in both instances the animals had a 100% penetrant *dcaf-1* germline nucleolus morphology defect (Table 1). This suggests that an increase in rRNA synthesis cannot rescue the nucleolus morphology defect.

FOG-1 inactivation suppresses the *dcaf-1* nucleolus morphology defect

When we initially approached this project, we focused on a previously described function of CRL4 in regulating DNA replication licensing in somatic cells (Zhong et al. 2003). We previously found that inactivation of core CRL4 components did not produce DNA re-replication in germ cells (Zhong et al. 2003; Kim and Kipreos 2007a) (see Supplementary Fig. 1). The CRL4 complex with the SR CDT-2 (*S. pombe* CDC10 dependent transcript homolog 2) prevents DNA re-replication in part by degrading the replication-licensing factor CDT-1 in S phase (Zhong et al. 2003). We did not observe a significant increase in CDT-1 in the germ line of *ddb-1* mutants (data not shown). However, to test if reducing CDT-1 levels by half would suppress the *ddb-1* germline nucleolus phenotype, we utilized a heterozygous genomic deletion, *qDf4*, that deletes approximately 1.1 genetic map units on chromosome I that includes the *cdt-1* gene. We observed that heterozygous *qDf4* gave a partial rescue of the *dcaf-1* RNAi phenotype (Table 1). However, *cdt-1* RNAi did not rescue the *dcaf-1(ok1867)* germline nucleolus defect, suggesting that another gene in the *qDf4* deletion region was responsible for the rescue.

There are 80 genes in the *qDf4* region. We focused on those genes that are expressed in the germ line (18 genes) (Wang et al. 2009) and had feeding-RNAi phenotypes (5 of the 18 genes). We tested these 5 genes (along with 14 other genes in the *qDf4* region) and found that only RNAi depletion of *fog-1* rescued the *dcaf-1* nucleolus phenotype (Supplementary Table 2). Several mutant alleles of *fog-1* (*q253ts*, *e2121*, *q325*, and *q241*) partially or fully suppress the *dcaf-1* RNAi nucleolus morphology phenotype, while allele *q372* does not (Table 1). The ability of the subset of *fog-1* alleles to rescue the *dcaf-1* RNAi phenotype is correlated with the mutations affecting all of the *fog-1* mRNA splice forms rather than only a subset. The *q253ts*, *e2121*, and *q325 fog-1* alleles that fully or partially rescue *dcaf-1* RNAi each inactivate all 4 splice isoforms of FOG-1 (2 long and 2 short isoforms) (wormbase, www.wormbase.org) (Table 1, Fig. 4a). In contrast, the *fog-1(q372)* allele, which inactivates only the 2 long isoforms of the *fog-1*, does not suppress the *dcaf-1* RNAi phenotype (Table 1). At least one short *fog-1* isoform, c, contains the 2 RNA recognition motif and zinc-finger C/H domains that are required in CPEB proteins to bind RNA (Hake et al. 1998). This suggests that either all *fog-1* isoforms must be inactivated to rescue the *dcaf-1* RNAi phenotype, or that the short isoforms, in particular, must be inactivated.

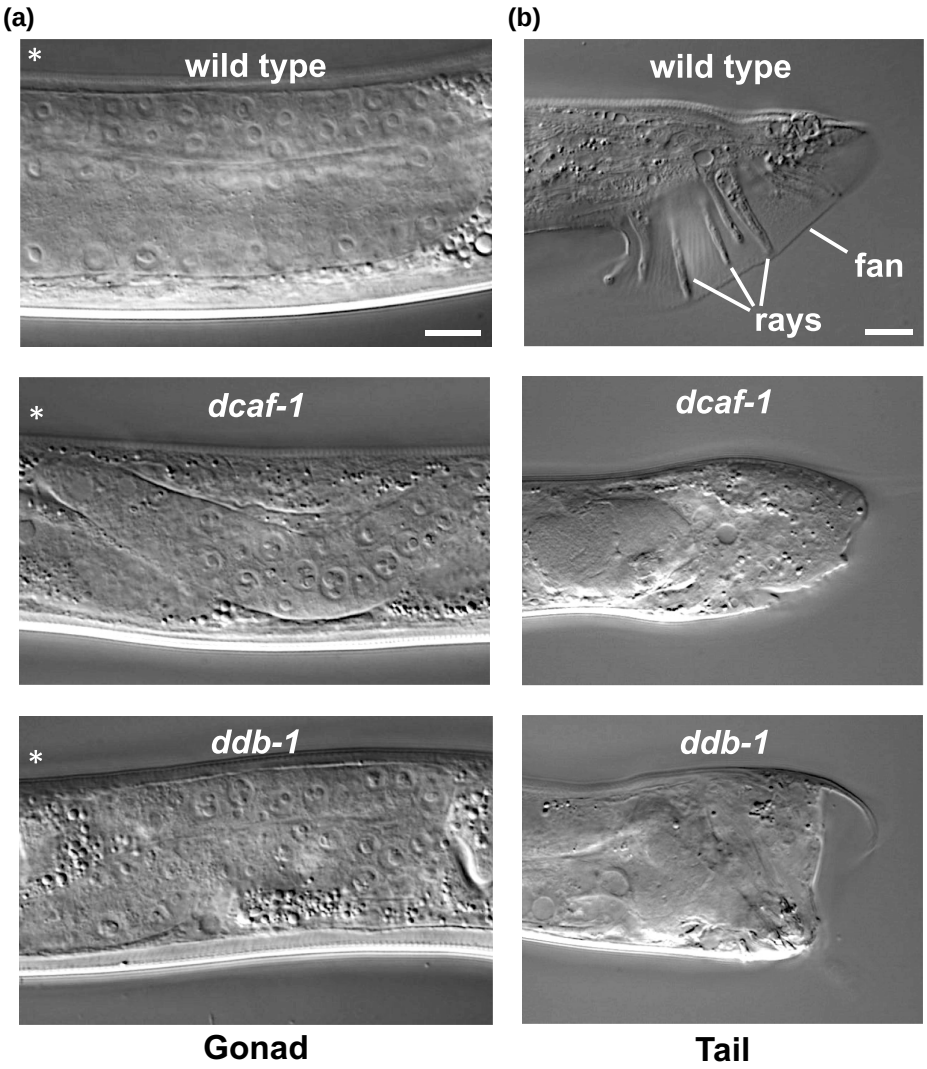

Fig. 3. *dcaf-1* and *ddb-1* mutant male tail and germ cell phenotypes. a) DIC micrographs of the distal end of the adult male germ line for wild type, *dcaf-1*(*ok1867*) mutant, and *ddb-1*(*tm1769*) mutant. The region with the distal end is denoted by an asterisk outside the body. b) DIC micrographs of the adult male tail for wild type, *dcaf-1* mutant, and *ddb-1* mutant. Sensory rays and fan are marked on the wild-type image (not all of the 9 rays per side are in focus in the DIC image). Rays and fans are not fully developed on *dcaf-1* and *ddb-1* mutant male tails. Scale bars, 10 μm.

Treating *dcaf-1* mutants with *fog-1* RNAi increases oocyte numbers substantially, from 23% of control (RNAi) hermaphrodites having oocytes ($n = 13$) to 91% of *fog-1(RNAi)* hermaphrodites having oocytes ($n = 11$). The *fog-1* RNAi is not fully penetrant and both wild type and *dcaf-1* mutants still produce sperm (which is absent in strong *fog-1* mutants). Notably, the *fog-1* RNAi rescues *dcaf-1* mutant sterility so that the *dcaf-1* mutants can reproduce for multiple generations (although in every brood, only a minority of the eggs hatch).

FOG-1 functions in a protein complex with the Tob/BTG family member FOG-3 (Ellis 2022). We observed partial suppression of the *dcaf-1* RNAi phenotype with 2 alleles of *fog-3* (Table 1). Alleles of 2 other genes that regulate sex determination, *fem-3* (loss-of-function) and *tra-1* (loss- and gain-of-function), did not rescue the *dcaf-1* germline defect (Table 1).

To determine whether the suppression of the *dcaf-1* nucleolus morphology defect by inactivation of *fog-1* and *fog-3* was associated with changes in the levels of FOG-1 and FOG-3 proteins, we utilized a strain that expresses single integrated copies of 3xMyc::FOG-1 and FOG-3::3xFLAG in a *fog-1* and *fog-3* mutant background (Noble et al. 2016). These transgenes are functional and rescue the *fog-1* and *fog-3* null mutant phenotypes (Noble et al. 2016). In wild-type genetic backgrounds, both FOG-1 and FOG-3 are restricted to the proximal region of late L3/early L4-stage animals (Noble et al. 2016). FOG-1 and FOG-3 germline expression ends in late L4-stage larvae and is absent from adult gonads (Lamont and Kimble 2007; Lee et al. 2011).

We analyzed the level of 3xMyc::FOG-1 and FOG-3::3xFLAG in dissected gonads of control RNAi and *dcaf-1* RNAi-treated adult hermaphrodites using immunofluorescence. Adults expressing 3xMyc::FOG-1 and FOG-3::3xFLAG that were treated with control RNAi did not have statistically higher Myc or FLAG signals relative to wild-type adults that do not express the transgenes and thus are negative controls for the staining (Fig. 4b and c). However, adults expressing 3xMyc::FOG-1 and FOG-3::3xFLAG that were treated with *dcaf-1* RNAi had Myc and FLAG signals that were significantly higher than the control in both the distal and proximal regions of the gonad (with the proximal region having higher levels) (Fig. 4b and c). Thus, when DCAF-1 is inactivated, both 3xMyc::FOG-1 and FOG-3::3xFLAG expression perdures into the

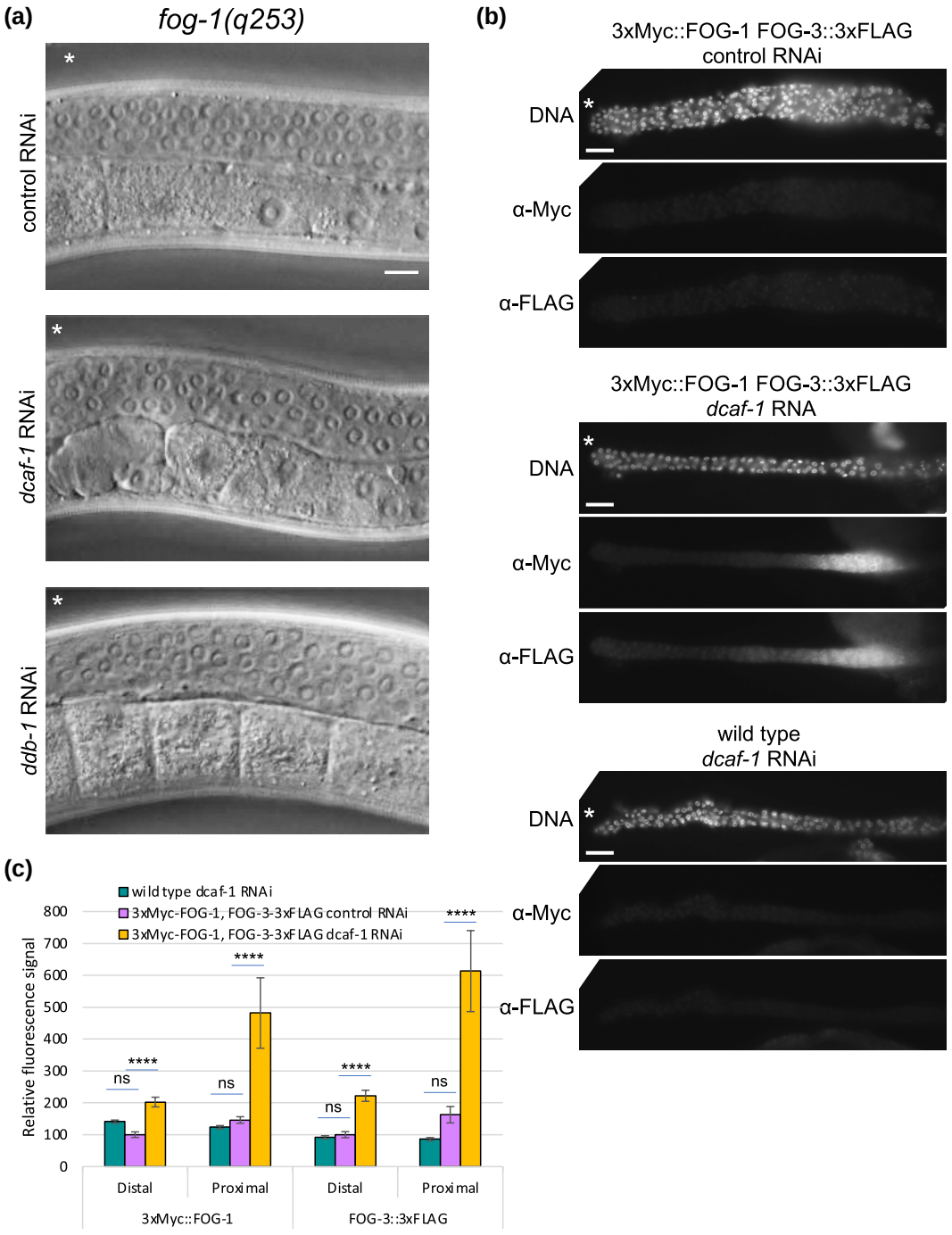

Fig. 4. FOG-1 inactivation rescues the *dcaf-1* germ cell defect and FOG-1 and FOG-3 levels increase in adult *dcaf-1(RNAi)* germ lines. a) DIC images of the germ line of *fog-1(q253ts)* mutant adults treated with control, *dcaf-1*, and *ddb-1* RNAi, and grown at 25°C. The distal region of the gonad is to the top left (marked by an asterisk). b) Immunofluorescence of dissected gonads stained with Hoechst 33258 DNA stain and anti-Myc and anti-FLAG antibodies in adults expressing 3xMyc-FOG-1 and FOG-3::3xFLAG treated with control RNAi (top) or *dcaf-1* RNAi (middle). Wild-type adults treated with *dcaf-1* RNAi (bottom) were used as a negative control for Myc and FLAG staining. The distal tip of the gonads is to the left (marked by an asterisk). Scale bars, 10 μm. c) Graph of the level of 3xMyc::FOG-1 and FOG-3::3xFLAG in the distal and proximal regions of the germ line of adults treated with control or *dcaf-1* RNAi.

adult stage, implying that DCAF-1 is required for the normal loss of FOG-1 and FOG-3 expression in wild-type adults. We did not observe a significant difference in the expression level of 3xMyc::FOG-1 and FOG-3::3xFLAG in L3/L4-stage larvae in proximal or distal regions of the gonad in response to *dcaf-1* RNAi (Supplementary Fig. 6).

PWP-1 is negatively regulated by CRL4^{DCAF-1} and reducing PWP-1 levels suppresses the *dcaf-1* mutant nucleolus defect

The ribosome assembly factor PWP1 is a substrate for CRL4^{DCAF1} in mice (Han et al. 2020). *C. elegans* has a single PWP1 ortholog with the cosmid designation JC8.2. JC8.2 and murine PWP1 share

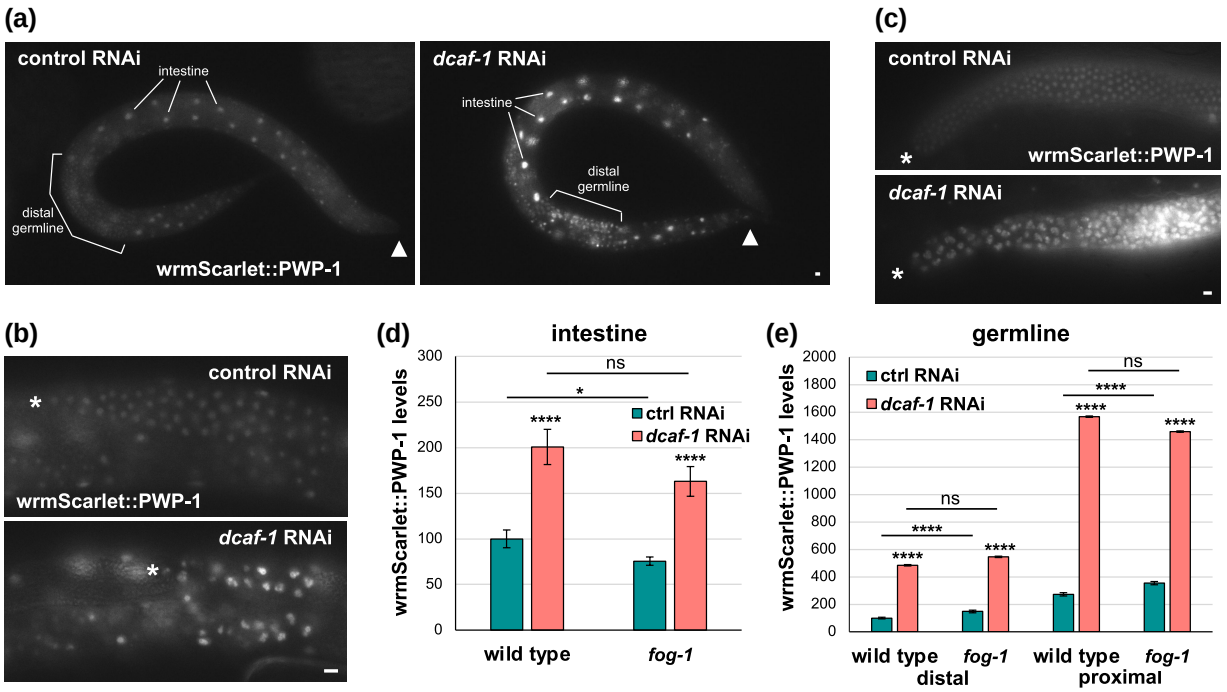

Fig. 5. PWP-1 levels are negatively regulated by CRL4^{DCAF-1}. a) wrmScarlet::PWP-1 levels in L4-stage larvae treated with control and *dcaf-1* RNAi from hatch. Note the increased levels of wrmScarlet::PWP-1 in the nucleoli of intestine cells and germ cells with *dcaf-1* RNAi. Arrowheads mark the anterior end of the animal. b) wrmScarlet::PWP-1 levels in gonad arms of L4-stage larvae treated with control and *dcaf-1* RNAi from hatch. c) wrmScarlet::PWP-1 levels in gonad arms of adults treated with control and *dcaf-1* RNAi for 3 days from the L3 larval stage. Asterisks mark the distal end of the germ line. Scale bars, 10 µm. d) Graph of wrmScarlet::PWP-1 levels in the intestine of wild type and *fog-1*(*q253ts*) mutant L4-stage larvae grown from hatching with control and *dcaf-1* RNAi. The level of wild-type larvae treated with control RNAi is set to 100. e) Graph of wrmScarlet::PWP-1 levels in the distal and proximal germ line of adult wild type and *fog-1*(*q253ts*) mutants were grown with control and *dcaf-1* RNAi from the L3-stage at 25°C for 3 days. The distal wild-type control RNAi level is set to 100. ns, not significant; *P-value < 0.05; ****P-value <0.0001. Statistics without lines refer to comparisons with the appropriate control RNAi.

37% amino acid sequence identity and reciprocally identify each other as the closest homolog in cross-species BLAST searches. Based on this orthology, we have named the *JC8.2* gene *pwp-1*.

The *pwp-1*(*ok3322*) allele is a deletion that eliminates 478 bp of genomic DNA including the 5′ splice site for the second intron. The deletion introduces a premature stop codon that eliminates 23.6% of the C-terminus of the PWP-1 protein (110 of 467 amino acids) (wormbase.org). *pwp-1*(*ok3322*) homozygotes arrest as young larvae, similar to *pwp-1*(*RNAi*) animals, suggesting that *ok3322* is a null allele (wormbase.org; data not shown).

We wanted to determine if CRL4^{DCAF-1} negatively regulates the level of PWP-1, as the orthologous CRL4^{DCAF1} complex does in mice. To follow PWP-1 protein levels, we introduced the wrmScarlet fluorescent protein (El Mouridi et al. 2017) into the N-terminus of the endogenous *pwp-1* locus using CRISPR/Cas9. Homozygous wrmScarlet::*pwp-1* animals develop normally to become healthy and fertile adults. This implies that the wrmScarlet::*pwp-1* fusion gene is able to accomplish all of the essential roles of the *pwp-1* gene. If the fusion gene did not function properly then we would expect an early larval arrest, as is observed for loss of *pwp-1*.

wrmScarlet::PWP-1 is enriched in nucleoli throughout the animal, including the nucleoli of cells in the hypodermis, intestine, and germ line (Fig. 5a, data not shown). Cells without obvious nucleoli, such as neurons, lack nuclear enrichment of PWP-1.

To determine if the inactivation of DCAF-1 increases wrmScarlet::PWP-1 levels, we subjected L4 larvae to control or *dcaf-1* RNAi, and analyzed their progeny, which had grown up in the presence of RNAi. We quantitated the level of wrmScarlet::PWP-1 in the intestine, germ line, and hypodermis of control vs *dcaf-1* RNAi-treated animals. The level of wrmScarlet::PWP-1 was substantially increased in the nucleoli of all 3 tissues upon treatment with *dcaf-1* RNAi. In the intestine, the level of wrmScarlet increased 2.1-fold upon *dcaf-1* RNAi compared to control RNAi in adults (Fig. 5a, d). In the germ line, we observed a 4.8-fold increase in wrmScarlet::PWP-1 for *dcaf-1* RNAi compared to control RNAi (Fig. 5b, 476 ± 0.07 vs 100 ± 0.46; n = 56 and 54, respectively). In the hypodermis, we observed a 2.8-fold increase in wrmScarlet::PWP-1 for *dcaf-1* RNAi compared to control RNAi (278 ± 11.7 vs 100 ± 2.9; n = 36 and 47, respectively).

The amount of wrmScarlet::PWP-1 in *dcaf-1*(*RNAi*) adult germ cells varied based on the nucleolus morphology with 3.4-fold higher levels in nucleoli with globular protrusions compared to nucleoli with a round morphology (n = 10 each, P-value <0.0001). Similar results were obtained in L4-stage germ cells with 2.6-fold higher wrmScarlet::PWP-1 levels in globular vs round nucleoli (n = 20 each, P-value <0.01). Therefore, the increase in PWP-1 levels correlates with aberrant nucleolus morphology.

Because the germ line of animals that were grown from hatching on *dcaf-1* RNAi is not developmentally normal, we wanted to determine if the increase in wrmScarlet::PWP-1 with *dcaf-1* RNAi occurs in a germ line that developed normally. We placed L3-stage larvae expressing wrmScarlet::PWP-1 (P0 stage) on *dcaf-1* RNAi and analyzed germ cells in the same (P0) adult animals 3 days later. In both the control and *dcaf-1* RNAi conditions, the level of wrmScarlet::PWP-1 was significantly higher in the proximal, pachytene region compared to the distal region (Fig. 5c, e). In the distal region, the level of wrmScarlet::PWP-1 was 4.8-fold higher with *dcaf-1* RNAi than with control RNAi (Fig. 5c, e). In the proximal region, the level of wrmScarlet::PWP-1 was 5.7-fold higher with *dcaf-1* RNAi than with control RNAi (Fig. 5c, e). These

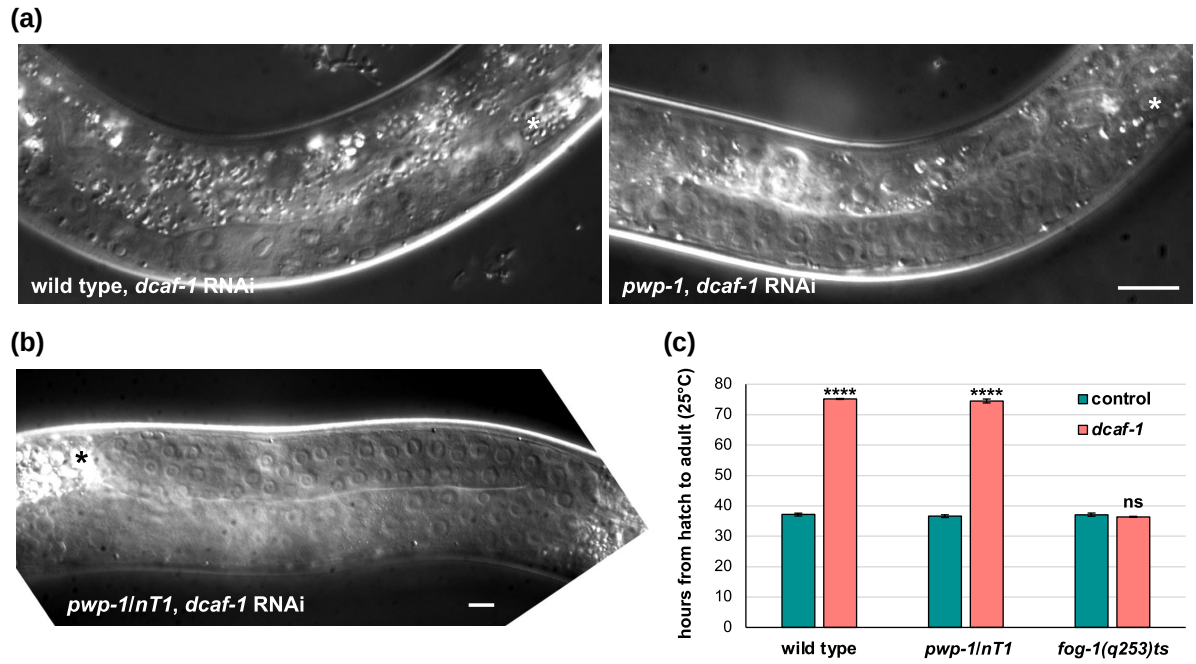

Fig. 6. PWP-1 inactivation rescues the *dcaf-1* RNAi germline nucleolus morphology defect but not the developmental delay, which is rescued by *fog-1* inactivation. a) Wild-type and homozygous *pwp-1*(*ok3322*) L2/L3-stage larvae treated with *dcaf-1* RNAi. The ventral side of the larvae is down. Note that wild type treated with *dcaf-1* RNAi has the germline nucleolus defect, with some cells that have normal morphology being somatic gonadal cells. The *pwp-1* homozygote treated with *dcaf-1* RNAi has normal nucleolus morphology in germ cells. b) *pwp-1*(*ok3322*)/*nT1* heterozygote L4-stage larvae grown on *dcaf-1* feeding-RNAi bacteria. Note the normal germ cell nucleolus morphology. Asterisks mark the distal end of the germ line. Scale bars, 10 µm. c) Graph of the timing of larval development from hatch to adult at 25°C for wild type, *pwp-1*(*ok3322*)/*nT1* heterozygotes, and *fog-1*(*q253ts*). Note that *dcaf-1* RNAi treatment induces a larval developmental delay in wild-type animals and heterozygous *pwp-1*/*nT1* mutants, but not in *fog-1*(*q253ts*) mutants.

results suggest that DCAF-1 negatively regulates the level of wrmScarlet::PWP-1 in diverse tissues including the germ line.

We wanted to determine if reducing the level of PWP-1 would rescue the *dcaf-1* mutant phenotype, as would be expected if the accumulation of PWP-1 contributed to the germline defects. *pwp-1*(*ok3322*) homozygotes and *pwp-1*(*RNAi*) animals undergo early larval arrest that would prevent our analysis of the germ line in later-stage larvae and adults. Therefore, we took 2 approaches to partially reduce PWP-1 activity to prevent early larval arrest. First, we used a heterozygous *pwp-1*(*ok3322*)/+ strain, which would be expected to halve the level of the endogenous PWP-1, and subjected this to control or *dcaf-1* RNAi. We found that 60% of the *pwp-1*/+ animals exhibited rescue of the *dcaf-1* RNAi germline defect, with 35% having a full rescue (no nucleolar defects) and 25% having a partial rescue (only a minority of germ cells with nucleolar defects) (Table 1, Fig. 6b). With the second approach, we diluted the bacteria expressing *pwp-1* dsRNA 1:1 with bacteria expressing control dsRNA to reduce the *pwp-1* RNAi effect. *dcaf-1*(*ok1867*) heterozygous L4-stage larvae were grown on 1:1 *pwp-1*:control feeding-RNAi bacteria and homozygous *dcaf-1*(*ok1867*) progeny were analyzed. The germline defect was rescued in 93% of the homozygous *dcaf-1*(*ok1867*) mutants (Table 1). When we analyze the germ line in *pwp-1* homozygotes treated with *dcaf-1* RNAi (which arrest as early larvae due to the homozygous *pwp-1*), we found that 100% were rescued for the *dcaf-1* germ cell morphology defect (Table 1, Fig. 6a). These results indicate that reducing PWP-1 levels rescues the *dcaf-1* germline nucleolus morphology defect.

Inactivation of *fog-1* does not reduce wrmScarlet::PWP-1 levels

Our study identified 3 genes whose inactivation suppresses the *dcaf-1* mutant germline defect: *pwp-1*, *fog-1*, and *fog-3* (which function together). A pertinent question is whether *fog-1* inactivation acts upstream of PWP-1 to prevent its accumulation. To test this, we compared the level of wrmScarlet::PWP-1 in an otherwise wild-type strain vs a strain with the *fog-1*(*q253ts*) allele. L4-stage larvae were placed on control or *dcaf-1* RNAi at the nonpermissive temperature of 25°C, and the level of wrmScarlet::PWP-1 was analyzed in the progeny. The level of wrmScarlet::PWP-1 in the intestine of *fog-1*(*q253ts*) young adults was increased 2.2-fold, which is similar to the 2.1-fold increase without the *fog-1* mutation (Fig. 5d). Placing *fog-1*(*q253ts*) L3-stage larvae grown at 25°C on *dcaf-1* RNAi and imaging the germ line after 3 days at 25°C showed a comparable increase in wrmScarlet::PWP-1 in both the distal and proximal germline regions compared to animals without functional FOG-1 (Fig. 5e). Thus, FOG-1 inactivation rescues the *dcaf-1* RNAi nucleolus phenotype through a mechanism that is independent of regulating PWP-1 levels.

Inactivation of *fog-1* suppresses *dcaf-1* RNAi developmental delay phenotype

dcaf-1 RNAi induces a severe developmental delay at 25°C (Fig. 5c). Intriguingly, homozygous *fog-1*(*q253ts*) mutation rescued the *dcaf-1* RNAi developmental delay at 25°C (Fig. 6c). In contrast, heterozygous *pwp-1* animals, which are partially resistant to the *dcaf-1* RNAi germline defect (Table 1), were as sensitive to the *dcaf-1* RNAi developmental delay as wild-type animals (Fig. 6c). These results suggest that inactivating FOG-1 prevents the *dcaf-1* mutant larval arrest phenotype, while this pathway is not affected by reducing PWP-1 levels.

Discussion

In this work, we identify DCAF-1 as the SR for a CRL4 complex that is required for proper germ cell nucleolus morphology and germ

cell numbers. Only a minority of *dcaf-1* mutants can form sperm or immature oocytes. This suggests that while entry into meiosis can still occur, it is limited, potentially by the significant reduction in germ cell proliferation. The mutants are invariably sterile and do not produce fully developed oocytes. Additionally, larval development is substantially delayed when DCAF-1 is inactivated.

The germ cell nucleolus defects are present in both hermaphrodites and males. However, males have an additional somatic defect in that the male tail is invariably deformed in adult *dcaf-1* and *ddb-1* mutants. Development of the male tail involves multiple transcription factors and signaling pathways that regulate the lineages that give rise to the cells and their subsequent development into the complex structures that make up the male tail (Emmons 2005). Understanding the reasons for the male tail morphology defect in *dcaf-1* mutants will require further study.

There is also a partially penetrant lethality of male *dcaf-1* embryos and larvae. The male *dcaf-1* lethality appears to be modified by the genetic background of the parental strain. The parental strain *dcaf-1*/*nT1* produces a higher percentage of arrested male *dcaf-1*/*dcaf-1* embryos than the parental strain *dcaf-1*(*ok1867*)/*lron-14*(*gk530*). The *nT1* translocation contains lethal mutation(s) that have not been identified, which may contribute to the increased *dcaf-1* male lethality.

The *C. elegans* sexes differ in their X-chromosome complement. Hermaphrodites are XX and males are XO. XO-specific lethality has previously been reported for loss-of-function mutations in the *xol-1* (XO lethal) gene (Miller et al. 1988). Loss of *xol-1* produces a fully penetrant lethality of XO animals as embryos or young larvae. The lethality is due to activating the hermaphrodite dosage compensation program in *xol-1* XO mutants, which reduces the expression of the single X chromosome by half (Meyer 2022). We do not know if the lethality of male *dcaf-1* and *ddb-1* mutants is due to a similar effect on dosage compensation or occurs through another pathway.

ncl-2 mutants show the same nucleolar morphology defect as the gene encoding the CRL4 adaptor, *ddb-1*, but the gene corresponding to the *ncl-2* mutant had not been molecularly identified. We determined that the *ncl-2* nucleolar morphology phenotype arises from a missense mutation in the *dcaf-1* coding region. Further, *dcaf-1* and *ncl-2* mutations fail to complement each other. Thus, *ncl-2* and *dcaf-1* are the same gene.

Analysis of transmission electron micrographs shows that *dcaf-1* mutant germ cells have reduced ribosome numbers, suggesting a defect in generating or maintaining normal ribosome numbers. The micrographs also show aberrations in the overall structure of the nucleolus with abnormal segregation of regions of different densities.

Bioanalyzer data does not show a difference in the relative proportions of 18S and 28S rRNAs in *dcaf-1*(*RNAi*) gonads. The total amount of rRNA was lower for the *dcaf-1*(*RNAi*) animals, but this is expected given that equivalent numbers of gonads were used and there are fewer germ cells per gonad with *dcaf-1* RNAi compared to control RNAi. Additionally, we observed a few differences in ribosomal subunit protein levels (that were 2-fold or less) in *dcaf-1*(*RNAi*) animals.

Our study shows that the levels of wrmScarlet::PWP-1 increase in the germ line, intestine, and hypodermis of *dcaf-1*(*RNAi*) animals, implying that $CRL4^{DCAF\text{-}1}$ negatively regulates PWP-1 levels in diverse tissues. Because PWP-1 is a direct substrate for $CRL4^{DCAF\text{-}1}$ in mammals, it is likely that it is also a direct substrate in *C. elegans*. The partial suppression of the *dcaf-1* mutant phenotype upon halving the genomic level of *pwp-1* in a heterozygote suggests that the increased expression of PWP-1 in *dcaf-1* mutants contributes to the nucleolus defect.

rRNA genes encode pre-rRNA that contains the 18S, 5.8S, and 28S rRNA that are separated by 2 internally transcribed spacers (ITS1 and ITS2). In *Drosophila* and human cells, PWP1 promotes rRNA transcription (Liu et al. 2017, 2018). In budding yeast, Pwp1p promotes the processing of pre-rRNA by removing the spacer ITS1 (Talkish et al. 2014). In human cells, knockdown of DCAF1 increases PWP1 levels and delays the cleavage at ITS1 (Han et al. 2020). However, the steady-state levels of the processed major rRNA bands (18S and 28S) are not affected by DCAF1 knockdown (Han et al. 2020) similar to what we have observed in *C. elegans* *dcaf-1*(*RNAi*) gonads.

The structure of the nucleolus is formed through liquid–liquid phase separation, wherein the interaction of components during rRNA transcription, rRNA processing, and ribosome assembly drives the self-association of those regions of the nucleolus (Lafontaine et al. 2021). Because this self-assembly depends on rRNA and ribosome processing occurring normally, defects in one or more of these steps would be expected to impact the overall nucleolar structure. A study that used siRNA to knockdown each ribosomal protein in human cells showed that many of the knockdowns produced radical changes in nucleolar morphology that are similar in severity to what is observed in *dcaf-1* mutants (Nicolas et al. 2016). It is possible that in *dcaf-1* mutants, defects in the processing of rRNA or rRNA transcription (both regulated by PWP1 in other species), or alterations in ribosomal protein levels (with the majority having reduced levels) affect aspects of ribosome assembly that generate the defect in nucleolar structure.

Inactivation of the mRNA-binding complex of FOG-1 and FOG-3 suppresses *dcaf-1* RNAi phenotypes in the germ line. We observed that the levels of FOG-1 and FOG-3 are increased in the germ lines of *dcaf-1*(*RNAi*) adults, a developmental stage when the 2 proteins are normally not present (Noble et al. 2016). However, we do not observe an increase in 3xMyc::FOG-1 or FOG-3::3xFLAG levels in the L3 or L4 larval stages of *dcaf-1*(*RNAi*) animals. We do not know if $CRL4^{DCAF\text{-}1}$ directly negatively regulates FOG-1 and FOG-3 levels in adult germ lines, or if their perdurance in *dcaf-1*(*RNAi*) animals is due to a secondary effect. Alterations of sex-determination pathway regulators are known to allow FOG-1 expression throughout adulthood, e.g. gain-of-function *fem-3* and *gld-1*(*Mog, masculinization of germline*) mutations, and loss-of-function *tra-1* and *fbf-1 puf-8* mutations (Lamont and Kimble 2007).

In the *C. elegans* germ line, FOG-1 and FOG-3 function together to repress oocyte development to thereby promote spermatogenesis during the L4 larval stage by regulating mRNA translation (Aoki et al. 2018; Ellis 2022). FOG-1 was found to physically associate with 81 mRNAs, the majority of which are also bound by FOG-3 (Noble et al. 2016). We did not identify published functional links to the nucleolus or ribosomes for the 81 genes whose mRNA are bound by FOG-1, although 39% of the genes have not been reported in the literature. The RNAi depletion of *fog-1* does not increase PWP-1 levels in control RNAi animals or further increases the elevated PWP-1 levels in *dcaf-1* RNAi animals. This suggests that the inactivation of *fog-1* rescues *dcaf-1* mutants independently of regulating PWP-1 levels. The mechanism by which loss of FOG-1 and FOG-3 rescues the germline defects of *dcaf-1* mutants is not known.

The *fem-3*(*e2006ts*) allele, a temperature-sensitive loss-of-function allele did not rescue the *dcaf-1* nucleolus defect at the nonpermissive temperature. On its surface, this is surprising because the inactivation of *fem* genes causes a reduction of FOG-1 levels (Lamont and Kimble 2007), which should rescue the *dcaf-1*

phenotype due to the reduction in FOG-1 levels. FEM-1, FEM-2, and FEM-3 function together in a ubiquitin-ligase complex that degrades TRA-1 (Starostina et al. 2007). FEM-1 and FEM-3 regulate the level of the large *fog-1* splice isoform mRNA, without affecting the mRNA level of the small *fog-1* isoform (Jin et al. 2001). The anti-FOG-1 antibody that was used to show that FOG-1 protein disappears in *fem-1* mutants was also specific for the long *fog-1* isoform (Thompson et al. 2005). We showed that *fog-1* mutations that only affected the long isoform do not rescue *dcaf-1* mutants. Thus, we assume that the inactivation of *fem-3* does not rescue the *dcaf-1* mutant phenotype because the short isoform of *fog-1* is still present. However, it has also been shown that the *fem* genes are required for *fog-3* mRNA expression (Chen and Ellis 2000). However, the extent that the inactivation of the *fem* genes alters the level of endogenous FOG-3 protein level has not been reported.

Interestingly, the inactivation of FOG-1 completely suppressed the larval developmental delay associated with *dcaf-1* RNAi, while a heterozygous *pwp-1* mutation had no effect on the developmental timing (despite suppressing the germline phenotype). This suggests that the developmental delay is mediated by the loss of a $CRL4^{DCAF\text{-}1}$ function that is independent of its negative regulation of PWP-1. The suppression of the developmental delay by the FOG-1 mutation is somewhat surprising because in the literature, FOG-1 function has only been described in the germ line, and the germ line has not been linked to larval developmental timing. A transcriptome analysis of somatic adult tissues showed somatic expression of FOG-1 in the hypodermis but not in the intestine, muscle, or neurons (Kaletsky et al. 2018). In *C. elegans*, the hypodermis is known to control the proliferation of cells in other tissues (Fukuyama et al. 2015). Potentially, the reduction of FOG-1 level in the hypodermis rescues the *dcaf-1* RNAi-mediated larval developmental delay. We did not observe a decrease in the number of ribosomes in the hypodermis of *dcaf-1(e1896)* animals, suggesting that differences in ribosome numbers are not involved in a potential role for the hypodermis in altering larval development in *dcaf-1* mutants. Currently, the molecular pathway by which loss of FOG-1 and FOG-3 suppresses the *dcaf-1* developmental timing defect is not known, and we cannot rule out that it may involve FOG-1 functioning in the germ line to affect signaling to the soma.

DCAF-1 is a conserved CRL4 SR that is present in both animals and plants (Zhang et al. 2008). Distinct CRL complexes often have evolutionarily conserved roles. For example, $CRL4^{CDT2}$ regulates DNA replication licensing in fission yeast, *C. elegans*, zebrafish, *Xenopus*, and humans (Kim and Kipreos 2007b), and $CRL4^{DDB2}$ regulates DNA repair in *Drosophila* and humans (Sun et al. 2010). Our finding that $CRL4^{DCAF\text{-}1}$ functions in *C. elegans* to regulate ribosome numbers and the ribosome assembly factor PWP-1, coupled with the finding that murine $CRL4^{DCAF1}$ also regulates PWP1, suggests an evolutionarily conserved role for $CRL4^{DCAF1}$ in regulating ribosome biogenesis. Interestingly, the *Drosophila* DCAF1 ortholog, Mahjong, has a similar phenotype to heterozygous mutations of ribosomal proteins in making cells susceptible to competition-induced cell loss (Baumgartner et al. 2021). Moreover, Mahjong mutant cells exhibit significantly reduced protein synthesis, which suggests a defect with ribosomes or their function (Nagata et al. 2019). Thus, considering all of the evidence, it appears that $CRL4^{DCAF1}$ has an ancestral role in regulating ribosome biogenesis in animals.

Data availability

Strains and plasmids are available upon request. The authors affirm that all data necessary for confirming the conclusions of the article are present within the article, figures, and tables.

Supplemental material available at GENETICS online

Acknowledgments

We acknowledge the late Nichol Thompson at the MRC LMB for his contributions to generating transmission electron micrographs. We thank Bronwyn E. Bennett for the purification of recombinant Cas9 protein from bacteria, which was used for CRISPR/Cas9 genome manipulations. We thank Mansi B. Patel for her help with image quantitation and figure preparation. We acknowledge the contributions of the Emory Integrated Proteomics Core, which performed the LC-MS/MS label-free quantification. Some strains were provided by the CGC, which is funded by the National Institutes of Health (NIH) Office of Research Infrastructure Programs (P40 OD010440). We also received strains from the National BioResource Project (NBRP) in Japan.

Funding

This work was supported by grantsm from the National Institute of General Medical Sciences of the NIH to ETK, R01GM074212 and R01GM134359.

Conflicts of interest

The author(s) declare no conflict of interest.

Literature cited

Aoki ST, Porter DF, Prasad A, Wickens M, Bingman CA, Kimble J. An RNA-binding multimer specifies nematode sperm fate. Cell Rep. 2018;23(13):3769–3775. doi:10.1016/j.celrep.2018.05.095.

Au V, Li-Leger E, Raymant G, Flibotte S, Chen G, Martin K, Fernando L, Doell C, Rosell FI, Wang S, *et al.* CRISPR/Cas9 methodology for the generation of knockout deletions in *Caenorhabditis elegans*. G3 (Bethesda). 2019;9(1):135–144. doi:10.1534/g3.118.200778.

Barton MK, Kimble J. fog-1, a regulatory gene required for specification of spermatogenesis in the germ line of *Caenorhabditis elegans*. Genetics. 1990;125(1):29–39. doi:10.1093/genetics/125.1.29.

Baumgartner ME, Dinan MP, Langton PF, Kucinski I, Piddini E. Proteotoxic stress is a driver of the loser status and cell competition. Nat Cell Biol. 2021;23(2):136–146. doi:10.1038/s41556-020-00627-0.

Chen P-J, Ellis RE. TRA-1A regulates transcription of fog-3, which controls germ cell fate in *C. elegans*. Development. 2000;127(14):3119–3129. doi:10.1242/dev.127.14.3119.

Chen D, Zhang Z, Li M, Wang W, Li Y, Wang W, Li Y, Rayburn ER, Hill DL, Wang H, *et al.* Ribosomal protein S7 as a novel modulator of p53-MDM2 interaction: binding to MDM2, stabilization of p53 protein, and activation of p53 function. Oncogene. 2007;26(35):5029–5037. doi:10.1038/sj.onc.1210327.

Cox J, Hein MY, Luber CA, Paron I, Nagaraj N, Mann M. Accurate proteome-wide label-free quantification by delayed normalization and maximal peptide ratio extraction, termed MaxLFQ. Mol Cell Proteomics. 2014;13(9):2513–2526. doi:10.1074/mcp.M113.031591.

Derenzini M, Trere D, Pession A, Govoni M, Sirri V, Chieco P. Nucleolar size indicates the rapidity of cell proliferation in cancer tissues. J Pathol. 2000;191(2):181–186. doi:10.1002/(SICI)1096-9896(200006)191:2<181::AID-PATH607>3.0.CO;2-V.

Ellis RE. Sex determination in nematode germ cells. Sex Dev. 2022; 16(5–6):305–322. doi:10.1159/000520872.

Ellis RE, Kimble J. The fog-3 gene and regulation of cell fate in the germ line of *Caenorhabditis elegans*. Genetics. 1995;139(2): 561–577. doi:10.1093/genetics/139.2.561.

El Mouridi S, Lecroisey C, Tardy P, Mercier M, Leclercq-Blondel A, Zariohi N, Boulin T. Reliable CRISPR/cas9 genome engineering in *Caenorhabditis elegans* using a single efficient sgRNA and an easily recognizable phenotype. G3 (Bethesda). 2017;7(5):1429–1437. doi:10.1534/g3.117.040824.

Emmons SW. Male development. In: WormBook, editor. The *C. elegans* Research Community, WormBook; 2005. p. 1–22. doi:10.1895/wormbook.1.33.1.

Feng H, Zhong W, Punkosdy G, Gu S, Zhou L, Seabolt EK, Kipreos ET. CUL-2 is required for the G1-to-S-phase transition and mitotic chromosome condensation in *Caenorhabditis elegans*. Nat Cell Biol. 1999;1(8):486–492. doi:10.1038/70272.

Frank DJ, Roth MB. ncl-1 is required for the regulation of cell size and ribosomal RNA synthesis in *Caenorhabditis elegans*. J Cell Biol. 1998;140(6):1321–1329. doi:10.1083/jcb.140.6.1321.

Fukuyama M, Kontani K, Katada T, Rougvie AE. The *C. elegans* hypodermis couples progenitor cell quiescence to the dietary state. Curr Biol. 2015;25(9):1241–1248. doi:10.1016/j.cub.2015.03.016.

Gartner A, Boag PR, Blackwell TK. Germline survival and apoptosis. In: WormBook, editor. The *C. elegans* Research Community, WormBook. 2008. p. 1–20. doi:10.1895/wormbook.1.145.1.

Gartner A, Engebrecht J. DNA Repair, recombination, and damage signaling. Genetics. 2022;220(2):1–41. doi:10.1093/genetics/iyab178.

Hake LE, Mendez R, Richter JD. Specificity of RNA binding by CPEB: requirement for RNA recognition motifs and a novel zinc finger. Mol Cell Biol. 1998;18(2):685–693. doi:10.1128/MCB.18.2.685.

Han XR, Sasaki N, Jackson SC, Wang P, Li Z, Smith MD, Xie L, Chen X, Zhang Y, Marzluff WF, *et al.* CRL4(DCAF1/VprBP) E3 ubiquitin ligase controls ribosome biogenesis, cell proliferation, and development. Sci Adv. 2020;6(51):1–12. doi:10.1126/sciadv.abd6078.

Henras AK, Soudet J, Gerus M, Lebaron S, Caizergues-Ferrer M, Mougin A, Henry Y. The post-transcriptional steps of eukaryotic ribosome biogenesis. Cell Mol Life Sci. 2008;65(15):2334–2359. doi:10.1007/s00018-008-8027-0.

Hodgkin J. Male phenotypes and mating efficiency in *Caenorhabditis elegans*. Genetics. 1983;103(1):43–64. doi:10.1093/genetics/103.1.43.

Hori Y, Engel C, Kobayashi T. Regulation of ribosomal RNA gene copy number, transcription and nucleolus organization in eukaryotes. Nat Rev Mol Cell Biol. 2023;24(6):414–429. doi:10.1038/s41580-022-00573-9.

Hubbard EJA, Schedl T. Biology of the *Caenorhabditis elegans* germline stem cell system. Genetics. 2019;213(4):1145–1188. doi:10.1534/genetics.119.300238.

Iarovaia OV, Minina EP, Sheval EV, Onichtchouk D, Dokudovskaya S, Razin SV, Vassetzky YS. Nucleolus: a central hub for nuclear functions. Trends Cell Biol. 2019;29(8):647–659. doi:10.1016/j.tcb.2019.04.003.

Jackson S, Xiong Y. CRL4s: the CUL4-RING E3 ubiquitin ligases. Trends Biochem Sci. 2009;34(11):562–570. doi:10.1016/j.tibs.2009.07.002.

Jin SW, Kimble J, Ellis RE. Regulation of cell fate in *Caenorhabditis elegans* by a novel cytoplasmic polyadenylation element binding protein. Dev Biol. 2001;229(2):537–553. doi:10.1006/dbio.2000.9993.

Kaletsky R, Yao V, Williams A, Runnels AM, Tadych A, Zhou S, Troyanskaya OG, Murphy CT. Transcriptome analysis of adult *Caenorhabditis elegans* cells reveals tissue-specific gene and isoform expression. PLoS Genet. 2018;14(8):e1007559. doi:10.1371/journal.pgen.1007559.

Kim J, Feng H, Kipreos ET. *C. elegans* CUL-4 prevents rereplication by promoting the nuclear export of CDC-6 via a CKI-1-dependent pathway. Curr Biol. 2007;17(11):966–972. doi:10.1016/j.cub.2007.04.055.

Kim Y, Kipreos ET. The *Caenorhabditis elegans* replication licensing factor CDT-1 is targeted for degradation by the CUL-4/DDB-1 complex. Mol Cell Biol. 2007a;27(4):1394–1406. doi:10.1128/MCB.00736-06.

Kim Y, Kipreos ET. Cdt1 degradation to prevent DNA re-replication: conserved and non-conserved pathways. Cell Div. 2007b;2(1):18. doi:10.1186/1747-1028-2-18.

Kipreos ET, van den Heuvel S. Developmental control of the cell cycle: insights from *Caenorhabditis elegans*. Genetics. 2019;211(3): 797–829. doi:10.1534/genetics.118.301643.

Kudron MM, Reinke V. *C. elegans* nucleostemin is required for larval growth and germline stem cell division. PLoS Genet. 2008;4(8): e1000181. doi:10.1371/journal.pgen.1000181.

Lafontaine DLJ, Riback JA, Bascetin R, Brangwynne CP. The nucleolus as a multiphase liquid condensate. Nat Rev Mol Cell Biol. 2021; 22(3):165–182. doi:10.1038/s41580-020-0272-6.

Lamont LB, Kimble J. Developmental expression of FOG-1/CPEB protein and its control in the *Caenorhabditis elegans* hermaphrodite germ line. Dev Dyn. 2007;236(3):871–879. doi:10.1002/dvdy.21081.

Lee MH, Kim KW, Morgan CT, Morgan DE, Kimble J. Phosphorylation state of a tob/BTG protein, FOG-3, regulates initiation and maintenance of the *Caenorhabditis elegans* sperm fate program. Proc Natl Acad Sci U S A. 2011;108(22):9125–9130. doi:10.1073/pnas.1106027108.

Lindstrom MS, Deisenroth C, Zhang Y. Putting a finger on growth surveillance: insight into MDM2 zinc finger-ribosomal protein interactions. Cell Cycle. 2007;6(4):434–437. doi:10.4161/cc.6.4.3861.

Liu Y, Cerejeira Matos R, Heino TI, Hietakangas V. PWP1 Promotes nutrient-responsive expression of 5S ribosomal RNA. Biol Open. 2018;7(11):1–4. doi:10.1242/bio.037911.

Liu Y, Mattila J, Ventela S, Yadav L, Zhang W, Lamichane N, Sundström J, Kauko O, Grénman R, Varjosalo M, *et al.* PWP1 Mediates nutrient-dependent growth control through nucleolar regulation of ribosomal gene expression. Dev Cell. 2017;43(2): 240–252.e5. doi:10.1016/j.devcel.2017.09.022.

Meyer BJ. The X chromosome in *C. elegans* sex determination and dosage compensation. Curr Opin Genet Dev. 2022;74:101912. doi:10.1016/j.gde.2022.101912.

Miller LM, Plenefisch JD, Casson LP, Meyer BJ. xol-1: a gene that controls the male modes of both sex determination and X chromosome dosage compensation in *C. elegans*. Cell. 1988;55(1): 167–183. doi:10.1016/0092-8674(88)90019-0.

Nagata R, Nakamura M, Sanaki Y, Igaki T. Cell competition is driven by autophagy. Dev Cell. 2019;51(1):99–112.e4. doi:10.1016/j.devcel.2019.08.018.

Nakagawa T, Mondal K, Swanson PC. VprBP (DCAF1): a promiscuous substrate recognition subunit that incorporates into both RING-family CRL4 and HECT-family EDD/UBR5 E3 ubiquitin ligases. BMC Mol Biol. 2013;14(1):22. doi:10.1186/1471-2199-14-22.

Neve IAA, Sowa JN, Lin CJ, Sivaramakrishnan P, Herman C, Ye Y, Han L, Wang MC. *Escherichia coli* metabolite profiling leads to the development of an RNA interference strain for *Caenorhabditis elegans*. G3 (Bethesda). 2020;10(1):189–198. doi:10.1534/g3.119.400741.

Nicolas E, Parisot P, Pinto-Monteiro C, de Walque R, De Vleeschouwer C, Lafontaine DLJ. Involvement of human ribosomal proteins in nucleolar structure and p53-dependent nucleolar stress. Nat Commun. 2016;7(1):11390. doi:10.1038/ncomms11390.

Noble DC, Aoki ST, Ortiz MA, Kim KW, Verheyden JM, Kimble J. Genomic analyses of sperm fate regulator targets reveal a

common set of oogenic mRNAs in *Caenorhabditis elegans*. Genetics. 2016;202(1):221–234. doi:10.1534/genetics.115.182592.

Poulin G, Nandakumar R, Ahringer J. Genome-wide RNAi screens in *Caenorhabditis elegans*: impact on cancer research. Oncogene. 2004;23(51):8340–8345. doi:10.1038/sj.onc.1208010.

Reddan JR, Unakar NJ. Electron microscopy of cultured mammalian lenses. II. Changes preceding and accompanying insulin-induced mitosis. Invest Ophthalmol. 1976;15(5):411–417. https://iovs.arvojournals.org/article.aspx?articleid=2175344

Reinke V, Gil IS, Ward S, Kazmer K. Genome-wide germline-enriched and sex-biased expression profiles in *Caenorhabditis elegans*. Development. 2004;131(2):311–323. doi:10.1242/dev.00914.

Starostina NG, Lim JM, Schvarzstein M, Wells L, Spence AM, Kipreos ET. A CUL-2 ubiquitin ligase containing three FEM proteins degrades TRA-1 to regulate *C. elegans* sex determination. Dev Cell. 2007;13(1):127–139. doi:10.1016/j.devcel.2007.05.008.

Sturm A, Saskői E, Tibor K, Weinhardt N, Vellai T. Highly efficient RNAi and cas9-based auto-cloning systems for *C. elegans* research. Nucleic Acids Res. 2018;46(17):e105. doi:10.1093/nar/gky516.

Sun NK, Sun CL, Lin CH, Pai LM, Chao CC. Damaged DNA-binding protein 2 (DDB2) protects against UV irradiation in human cells and Drosophila. J Biomed Sci. 2010;17(1):27. doi:10.1186/1423-0127-17-27.

Talkish J, Campbell IW, Sahasranaman A, Jakovljevic J, Woolford JL Jr. Ribosome assembly factors pwp1 and Nop12 are important for folding of 5.8S rRNA during ribosome biogenesis in *Saccharomyces cerevisiae*. Mol Cell Biol. 2014;34(10):1863–1877. doi:10.1128/MCB.01322-13.

Thompson BE, Bernstein DS, Bachorik JL, Petcherski AG, Wickens M, Kimble J. Dose-dependent control of proliferation and sperm specification by FOG-1/CPEB. Development. 2005;132(15):3471–3481. doi:10.1242/dev.01921.

Timmons L, Court DL, Fire A. Ingestion of bacterially expressed dsRNAs can produce specific and potent genetic interference in *Caenorhabditis elegans*. Gene. 2001;263(1–2):103–112. doi:10.1016/S0378-1119(00)00579-5.

Uppaluri S, Weber SC, Brangwynne CP. Hierarchical size scaling during multicellular growth and development. Cell Rep. 2016;17(2):345–352. doi:10.1016/j.celrep.2016.09.007.

Voutev R, Killian DJ, Ahn JH, Hubbard EJ. Alterations in ribosome biogenesis cause specific defects in *C. elegans* hermaphrodite gonadogenesis. Dev Biol. 2006;298(1):45–58. doi:10.1016/j.ydbio.2006.06.011.

Wang X, Zhao Y, Wong K, Ehlers P, Kohara Y, Jones SJ, Marra MA, Holt RA, Moerman DG, Hansen D. Identification of genes expressed in the hermaphrodite germ line of *C. elegans* using SAGE. BMC Genomics. 2009;10(1):213. doi:10.1186/1471-2164-10-213.

Yuan X, Zhou Y, Casanova E, Chai M, Kiss E, Gröne H-J, Schütz G, Grummt I. Genetic inactivation of the transcription factor TIF-IA leads to nucleolar disruption, cell cycle arrest, and p53-mediated apoptosis. Mol Cell. 2005;19(1):77–87. doi:10.1016/j.molcel.2005.05.023.

Zhang Y, Feng S, Chen F, Chen H, Wang J, McCall C, Xiong Y, Deng XW. Arabidopsis DDB1-CUL4 ASSOCIATED FACTOR1 forms a nuclear E3 ubiquitin ligase with DDB1 and CUL4 that is involved in multiple plant developmental processes. Plant Cell. 2008;20(6):1437–1455. doi:10.1105/tpc.108.058891.

Zhong W, Feng H, Santiago FE, Kipreos ET. CUL-4 ubiquitin ligase maintains genome stability by restraining DNA-replication licensing. Nature. 2003;423(6942):885–889. doi:10.1038/nature01747.

Zhou Z, Song X, Wavelet CM, Wan Y. Cullin 4-DCAF proteins in tumorigenesis. Adv Exp Med Biol. 2020;1217:241–259. doi:10.1007/978-981-15-1025-0_15.

Zou L, Wu D, Zang X, Wang Z, Wu Z, Chen D. Construction of a germline-specific RNAi tool in *C. elegans*. Sci Rep. 2019;9(1):2354. doi:10.1038/s41598-019-38950-8.

Editor: B. Grant